

27. ROCK MAGNETIC PROPERTIES, MAGNETIC MINERALOGY, AND MAGNETIC FABRIC OF ROCKS IN THE D'ENTRECASTEAUX COLLISION ZONE¹

L.B. Stokking,^{2,3} D. Merrill,³ X. Zhao,⁴ and P. Roperch⁵

ABSTRACT

During Leg 134, the influence of ridge collision and subduction on the structural evolution of island arcs was investigated by drilling at a series of sites in the collision zone between the d'Entrecasteaux Zone (DEZ) and the central New Hebrides Island Arc. The DEZ is an arcuate Eocene-Oligocene submarine volcanic chain that extends from the northern New Caledonia Ridge to the New Hebrides Trench. High magnetic susceptibilities and intensities of magnetic remanence were measured in volcanic silts, sands, siltstones, and sandstones from collision zone sites. This chapter presents the preliminary results of studies of magnetic mineralogy, magnetic properties, and magnetic fabric of sediments and rocks from Sites 827 through 830 in the collision zone. The dominant carrier of remanence in the highly magnetic sediments and sedimentary rocks in the DEZ is low-titanium titanomagnetite of variable particle size. Changes in rock magnetic properties reflect variations in the abundance and size of titanomagnetite particles, which result from differences in volcanogenic contribution and the presence or absence of graded beds. Although the anisotropy of magnetic susceptibility results are difficult to interpret in terms of regional stresses because the cores were azimuthally unoriented, the shapes of the susceptibility ellipsoids provide information about deformation style. The magnetic fabric of most samples is oblate, dominated by foliation, as is the structural fabric. The variability of degree of anisotropy (P) and a factor that measures the shape of the ellipsoid (q) reflect the patchy nature of deformation, at a micrometer scale, that is elucidated by scanning electron microscope analysis. The nature of this patchiness implies that deformation in the shear zones is accomplished primarily by motion along bedding planes, whereas the material within the beds themselves remains relatively undeformed.

INTRODUCTION

During Leg 134, the influence of ridge collision and subduction on the structural evolution of island arcs was investigated by drilling at a series of sites in the collision zone between the d'Entrecasteaux Zone (DEZ) and the central New Hebrides Island Arc (Figs. 1 and 2). The DEZ is an arcuate Eocene-Oligocene submarine volcanic chain extending from the northern New Caledonia Ridge to the New Hebrides Trench. Near the New Hebrides Trench, the DEZ comprises two parallel morphologic features that trend east-west: the fairly continuous North d'Entrecasteaux Ridge (NDR) and the South d'Entrecasteaux Chain (SDC), which are composed of seamounts and guyots. The impingement of the DEZ upon the central New Hebrides Island Arc has greatly disrupted and tectonically modified arc morphology and structure. Holes at Sites 827 and 829 were drilled to penetrate the lowermost accretionary wedge and the interplate thrust fault (décollement), where the NDR collides with the New Hebrides Island Arc. The primary objective of drilling at Site 828 was to obtain a reference section of rocks from the north ridge. Holes at Site 830 were drilled to penetrate imbricated arc rocks in the collision zone between the Bougainville Guyot (eastern member of the SDC) and the arc.

Preliminary interpretations of the results of Leg 134 suggest that each ridge of the twin-ridge DEZ causes different forearc deformation. The sedimentary and surficial basement rocks of the NDR, whose basement rocks (mid-ocean ridge basalts, or MORBs) are denser than those of the Bougainville Guyot, appear to have been scraped off and accreted to the forearc during subduction (Collot et al., this volume; Fisher et al., 1986; Greene et al., this volume). This accretion has

formed the Wousi Bank, which consists of uplifted forearc rocks and stacked thrust sheets. The SDC impacts the forearc in a different manner: little deformational uplift, but considerable indenting, has occurred compared to the NDR collision zone, although the SDC is converging at the same rate and at the same angle as the NDR (Collot, Greene, Stokking, et al., 1992).

This chapter presents the preliminary results of studies of magnetic mineralogy, magnetic properties, and magnetic fabric of sediments and rocks from Sites 827 through 830 in the collision zone. Additional work on these units is presented in two chapters by Roperch et al. (this volume).

LITHOSTRATIGRAPHY

Drilling results are presented in Collot, Greene, Stokking, et al. (1992), Reid et al. (this volume), and are summarized in Table 1. Typical sediments and rocks are illustrated in Plate 1. Drilling at Site 827 (Figs. 1 and 2) recovered primarily arc-derived turbiditic volcanic silts and silty sands. At Site 828 on the NDR drilling recovered high-susceptibility volcanic silts in the upper part of Hole 828A and primarily low-susceptibility oozes and chalks in Hole 828B.

At Site 829 collision has formed an accretionary complex that is at least 590 m thick at a distance of 2 km from the trench (Figs. 1 and 2). Site 829 contains 21 lithostratigraphic units, several of which represent repeated lithologies. Because of these repetitions, during Leg 134 the lithostratigraphic units were divided into four composite units (Bigwan Wan, Bigwan Tu, Bigwan Tri, and Bigwan Fo, named in Bislama, the official language of the Republic of Vanuatu; Collot, Greene, Stokking, et al., 1992). These composite units have been defined on the basis of age and lithologies. Bigwan Wan comprises Pleistocene volcanic silt, sandstone, and gray silty chalk. Bigwan Tu contains upper Oligocene to lower Miocene foraminiferal and calcareous chalk. Bigwan Tri is an upper Pliocene or Pleistocene chalk breccia with upper Oligocene to lower Miocene clasts. Bigwan Fo is a breccia of unknown age with clasts of basaltic rock fragments, microgabbros, and gabbros. Lithostratigraphic units are numbered consecutively starting with Hole 829A and ending with Hole 829C.

¹ Greene, H.G., Collot, J.-Y., Stokking, L.B., et al., 1994. *Proc. ODP, Sci. Results*, 134: College Station, TX (Ocean Drilling Program).

² ODP, College Station, TX 77845-9547, U.S.A.

³ Department of Geophysics, Texas A&M University, College Station, TX 77843, U.S.A.

⁴ Earth Sciences Board, University of California, Santa Cruz, CA 95064, U.S.A.

⁵ Laboratoire de Géodynamique Sous-Marine, Centre d'Études et de Recherches Océanographiques de Villefranche-sur-Mer, B.P. 48, 06230, Villefranche-sur-Mer, France.

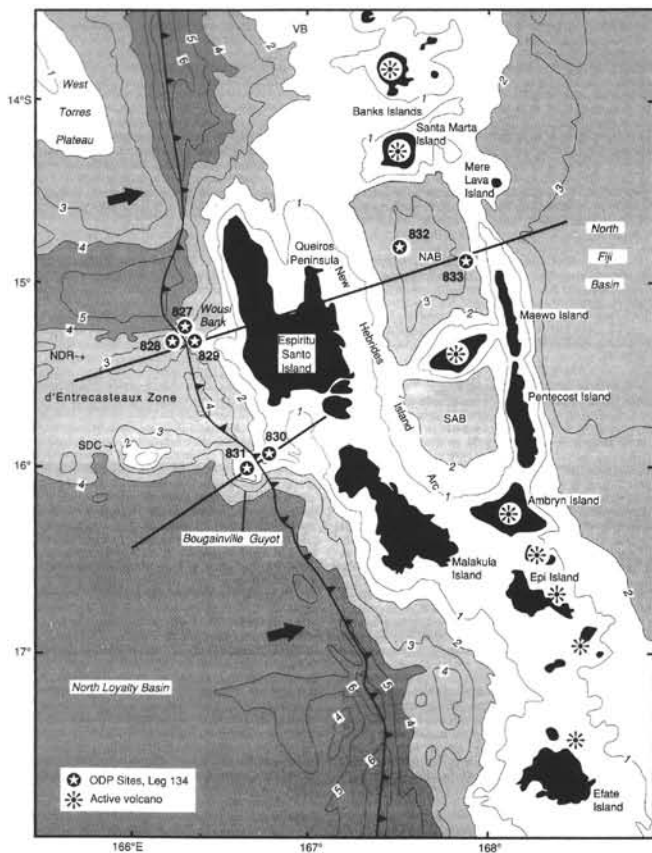


Figure 1. The d'Entrecasteaux Zone-central New Hebrides Island Arc collision zone. Bathymetry (in kilometers) after Kroenke et al. (1983). NDR = North d'Entrecasteaux Ridge, NAB = North Aoba Basin, SAB = South Aoba Basin.

Initial interpretations of cores suggest that many of the units identified in Hole 829A are similar to those observed in Hole 828A. For example, the calcareous chalk and pale brown chalk of Bigwan Tu are similar in age and lithology to the nannofossil chalk of lithostratigraphic Unit II from Hole 828A. Igneous rocks collected at both Sites 828 and 829 are similar. Therefore the Leg 134 shipboard party (Collot, Greene, Stokking, et al., 1992) and post-cruise researchers (Collot et al., this volume; Greene et al., this volume; and Reid, et al., this volume) concluded that an accretionary prism, composed in part of offscraped rocks and sediments from the downgoing NDR, was penetrated at Site 829.

Site 830 was drilled on the forearc slope in a gently eastward-dipping thrust sheet. Rocks recovered include very coarse, cataclastic volcanoclastic sandstones that are similar in composition to rocks exposed on nearby Espiritu Santo and Malakula islands (Mitchell and Warden, 1971; Mallick and Greenbaum, 1977).

METHODS

Two-hundred-nine samples were studied (Table 2). The set included 130 samples of volcanic silts and siltstones, 40 volcanic sands and sandstones, 12 breccias and conglomerates, 19 oozes and chinks, and eight samples of mixed sediment and sedimentary rocks.

Magnetic hysteresis is measured by applying an increasing magnetic field to a sample, then reversing the applied field, while continuously measuring the magnetization of the sample as it responds to the changing applied field. A plot of applied field vs. sample magnetization results in a loop, the shape of which is determined by the chemical composition, microstructure, and particle orientation of the magnetic material within the sample (Stacey and Banerjee, 1974; Day et al.,

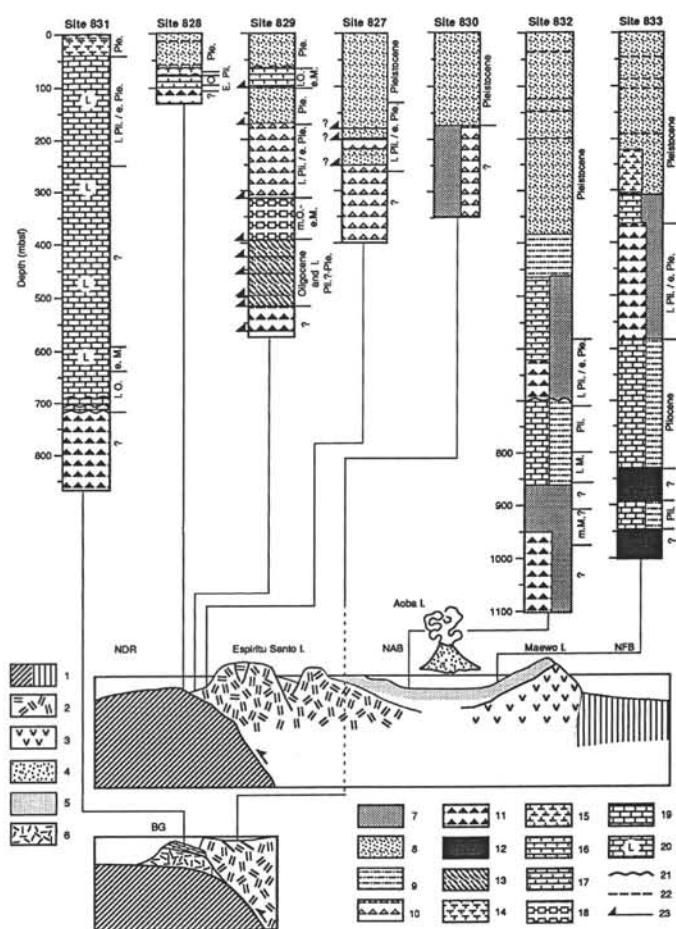


Figure 2. East-west cross sections of the collision zone with projected simplified lithologic columns. Location of cross sections is shown in Figure 1. Legend is as follows: 1. Oceanic crust, 2. Western Belt volcanic rocks, 3. Eastern Belt volcanic rocks, 4. Central Chain volcanic rocks, 5. Basin fill, 6. Guyot volcanic rocks, 7. Volcanic sand/sandstone, 8. Volcanic silt/siltstone, 9. Volcanic sandstone/siltstone/claystone, 10. Sed-lithic breccia, 11. Volcanic breccia, 12. Basalt, 13. Multiple slivers of siltstone and chalk, 14. Foraminiferal ooze, 15. Nannofossil ooze, 16. Foraminiferal chalk, 17. Nannofossil chalk, 18. Calcareous chalk, 19. Pelagic limestone, 20. Lagoonal limestone, 21. Unconformity, 22. Ash, 23. Thrust fault; l. Pli./e. Ple is late Pliocene or early Pleistocene, l. O.-e. M. is late Oligocene to early Miocene, E. is Eocene, m.M. is middle Miocene, NDR is North d'Entrecasteaux Ridge, BG is Bougainville Guyot, NAB is North Aoba Basin, NFB is North Fiji Basin.

1977; Cisowski, 1980; O'Reilly, 1984). Measurement of magnetic hysteresis can provide information about several rock magnetic properties: coercivity (H_C), saturation remanence (M_{RS}), and saturation magnetization (M_S). These parameters, in conjunction with coercivity of remanence (H_{CR}), then provide constraints on the domain state of the magnetic minerals in the sample (Dunlop, 1969). Domain state is in turn related to particle size (see "Discussion" section, this chapter). Hysteresis behavior of nine samples was measured using a Princeton Applied Research vibrating sample magnetometer housed in the Physics Department at the University of California, Davis.

Magnetic susceptibility provides information about the type and concentration of remanence-carrying minerals (such as titanomagnetite) in a sample. Magnetic susceptibilities of the archive halves of cores were measured on board ship using a Bartington Instruments magnetic susceptibility meter (model MS1) with an 80-mm sensor loop at a frequency of 0.47 kHz. Magnetic susceptibilities of 209 discrete samples were measured at TAMU using a Bartington Instru-

Table 1. Lithologic summary of Sites 827, 828, 829, and 830.

Lithologic unit	Lithologic subunit	Core, section, interval (cm)	Depth (mbsf)	Thickness (m)	Dominant lithology	Age	
Site 827	I	827A-1H-1, 0 to -13H-1, 60	0.0-88.4	88.4	Volcanic silt, volcanic silty sand	Pleistocene	
		827A-1H-1, 0 to -3H-6, 150	0.0-27.0	27.0	Few graded interbeds	Pleistocene	
		827A-3H-6, 150 to -8H-4, 50	27.0-66.0	39.0	Several graded interbeds	Pleistocene	
		827A-8H-4, 50 to -13H-6, 60	66.0-88.4	22.4	Few graded interbeds	Pleistocene	
	II	827A-13H-6, 60 to -827B-4R-3, 90	88.4-141.0	52.6	Volcanic silt and siltstone	Pliocene to Pleistocene	
	III	827B-4R-3, 90 to -15R-CC, 15	141.0-252.6	111.0	Calcareous volcanic siltstone, sed-lithic conglomerate	Pliocene to Pleistocene	
	IV	IIIA	827B-4R-3, 90 to -10R-4, 120	141.0-200.0	59.0	Volcanic siltstone	Pleistocene
		IIIB	827B-10R-4, 120 to -12R-3, 90	200.0-218.0	18.0	Sed-lithic conglomerate and breccia	Pliocene or Pleistocene
		IIIC	827B-12R-3, 90 to -15R-CC, 15	218.0-252.6	34.6	Volcanic siltstone	Pliocene
	IV	827B-15R-CC, 15 to -31R-CC, 7	252.6-400.4	147.8	Volcanic siltstone and sandstone, breccia	Barren	
Site 828	I	828A-1H-1, 0 to -8H-1, 48	0.0-61.9	61.9	Volcanic silt, volcanic sandy silt	Pleistocene	
	II	828A-8H-1, 48 to -8H-6, 42	61.9-69.3	7.4	Foraminiferal ooze	Pleistocene, Pliocene	
	III	828A-8H-6, 42 to -11H-1, 92	69.3-90.8	21.5	Nannofossil chalk	Oligocene	
	III	828B-1R-1, 0 to -2R-1, 0	90.0-100.0	10.0	Nannofossil chalk	Oligocene/Eocene	
	IV	828A-11H-1, 92 to -15N-2, 185	90.8-111.4	20.6	Volcanic breccia	Eocene(?)	
IV	828B-2R-1, 0 to -3R-1, 12	100.0-119.4	19.4	Volcanic breccia	Barren		
Hole 829A	I	829A-1R-1, 0 to -8R-1, 0	0-60.5	60.5	Clayey volcanic silt	Pleistocene	
	II	829A-8R-1, 0 to -12R-1, 40	60.5-99.4	38.9	Foraminiferal chalk	late Oligocene to early Miocene	
	III	829A-12R-1, 40 to -19R-4, 88	99.4-171.9	72.5	Clayey volcanic silt	Pleistocene	
	IV	829A-19R-4, 88 to -23R-1, 0	171.9-205.2	33.3	Siltstone-chalk breccia	Pleistocene	
	V	829A-23R-1, 0 to -41R-1, 0	205.2-378.4	173.2	Chalk breccia	late Pliocene or Pleistocene	
	VI	829A-41R-1, 0 to -43R-1, 120	378.4-398.9	20.5	Calcareous chalk	Oligocene and Eocene	
	VII	829A-43R-1, 120 to -43R-CC, 20	398.9-406.0	7.1	Volcanic breccia, clayey chalk	Indeterminate, Eocene	
	VIII	829A-43R-CC, 20 to -44R-1, 40	406.0-413.0	7.0	Foraminiferal chalk	early Pliocene	
	IX	829A-44R-1, 40 to -45R-CC, 5	413.0-419.6	6.6	Silty chalk	Pleistocene	
	X	829A-45R-CC, 5 to -47R-1, 65	419.6-435.0	15.4	Calcareous chalk and foraminiferal chalk	Oligocene or Miocene	
	XI	829A-47R-1, 65 to -48R-CC, 12	435.0-442.0	7.0	Silty chalk	Pliocene (?) and Pleistocene	
	XII	829A-48R-CC, 12 to -51R-3, 10	442.0-463.2	2.2	Calcareous chalk	Oligocene to Miocene	
	XIII	829A-51R-3, 10 to -54R-1, 0	463.2-484.5	21.3	Volcanic sandstone	Pliocene or Pleistocene	
	XIV	829A-54R-1, 0 to -55R-CC, 15	484.5-495.6	11.1	Chalk and mixed sediment	Oligocene or Miocene	
	XV	829A-55R-CC, 15 to -57R-3, 72	495.6-517.2	21.6	Sandy volcanic siltstone	Pliocene to Pleistocene	
	XVI	829A-57R-3, 72 to -64R-CC, 27	517.2-590.3	73.1	Igneous sed-lithic breccia	Eocene	
Hole 829B	XVII	829B-1H-1, 0 to -3H-CC, 50	0.0-19.5	19.5	Clayey sandy volcanic silt	Pleistocene	
Hole 829C	XVIII	829C-1H-1, 0 to -9H-4, 0	0.0-54.6	54.6	Clayey sandy volcanic silt	Pleistocene	
	XIX	829C-9H-4, 0 to -10H-1, 0	4.6-57.3	2.7	Foraminiferal ooze	early Miocene	
	XX	829C-10H-1, 0 to -11H-1, 0	57.3-58.3	1.0	Foraminiferal silty mixed sediment	Pleistocene	
	XXI	829C-11H-1, 0 to -11H-CC, 15	58.3-58.4	0.1	Foraminiferal chalk	Pleistocene	
Site 830	I	830A-1H-1, 0 to -11X-1, 34	0.0-96.9	96.9	Volcanic silt and volcanic siltstone	Pleistocene	
		830A-1H-1, 0 to -3H-3, 150	0.0-21.0	21.0	Volcanic silt	Pleistocene	
		830A-3H-4, 0 to -6H-5, 110	21.0-47.0	26.0	Volcanic sand interbeds	Pleistocene	
		830A-6H-5, 110 to -11X-1, 34	47.0-96.9	49.9	Interbedded sandy silts and silty sands	Pleistocene	
	IC	830B-1R-1, 0 to -14R-1, 0	48.5-174.9	126.4	Interbedded sandy silts and silty sands	Pleistocene	
	II	830B-14R-1, 0 to -24R-CC, 15	174.9-281.7	106.8	Volcanic sed-lithic sandstone	Barren	
II	830C-1R-1, 0 to -12R-CC, 14	235.0-350.6	115.6	Volcanic sed-lithic sandstone	Barren		

ments susceptibility meter, model MS2, at a frequency of 0.47 kHz. Data are reported as volume susceptibility (k).

Whole-rock samples from shear zones were observed using a JEOL JSM 6400 scanning electron microscope (SEM) with Tracor Northern, Series 2, energy-dispersive X-ray analysis. Magnetic separates of volcanic silt (Samples 134-827A-9H-1, 118 cm, and -829A-6R-4, 110 cm) prepared by attracting particles in a slurry of ultrasonically suspended sediment and deionized water to a magnet, were also analyzed.

Alternating field (AF) demagnetization of the natural remanent magnetization (NRM) of a sample provides information about its coercivity spectrum, a property that, assuming the sample contains a single type of magnetic carrier, is itself dependent on the range of sizes of magnetic particles in the rock. Aboard ship, both a 2-G Enterprises (Model 760R) pass-through cryogenic rock magnetometer and a Mol-spin spinner magnetometer were used to measure NRM. At TAMU,

NRM intensities were measured using a three-axis CTF cryogenic magnetometer housed in a shielded room in the Paleomagnetism Laboratory at the Department of Geophysics. An AF demagnetizer (Model 2G600) capable of producing a peak field up to 20 Mt was used on-line with the pass-through cryogenic magnetometer on board ship. Ship-board AF demagnetization at higher fields and AF demagnetization at TAMU were performed using a single-axis Schonstedt geophysical specimen demagnetizer (Model GSD-1) capable of producing peak fields up to 100 mT. Exposure to strong magnetic fields in the core barrel, in the steel drill pipe, and on the rig floor impart a steep negative inclination to cores, particularly those containing low-coercivity material. The intensity of the overprint decreases radially from the edge of the core to its center; thus samples taken from the center of the core are less affected than those from the edge (Collot, Greene, Stokking, et al., 1992). This spurious magnetization was removed from most Leg

Table 2. List of samples, depths, lithologic information, rock magnetic data. Acronyms and abbreviations are defined in the text.

Sample	Depth (mbsf)	Lithology	NRM (A/m)	RM ₁₀ (A/m)	MDF (mT)	IRM ₁₀₀₀ (A/m)	ARM ₁₀₀ (A/m)	K (SI)	Sample	Depth (mbsf)	Lithology	NRM (A/m)	RM ₁₀ (A/m)	MDF (mT)	IRM ₁₀₀₀ (A/m)	ARM ₁₀₀ (A/m)	K (SI)
Hole 827A									3H-3, 49	13.5	Silt	0.29	0.03	5	94.17	3.14	0.004
9H-1, 118	68.2	Volc. silt	0.60	0.16	5	120.66	2.15	0.0083	3H-4, 58	15.1	Silt	0.61	0.16	5	99.66	2.79	0.0046
9H-2, 83	69.3	Volc. silt	0.62	0.12	3	137.43	3.68	0.0041	3H-5, 68	16.7	Silt	1.24	0.17	30	106.03	3.57	0.0039
11H-4, 75	82.9	Volc. silt	0.19	0.12	15	109.81	2.52	0.0051	Hole 829C								
Hole 827B									1H-2, 32	1.8	Silt	0.36	0.12	5	141.21	2.85	0.0071
5R-1, 4	146.5	Siltst.	0.06	0.04	20	79.65	1.84	0.0028	1H-3, 43	3.4	Silt	0.25	0.11	7	111.41	2.98	0.0038
5R-3, 86	150.4	Sndst.	0.12	0.04	7.5	108.25	2.48	0.0032	1H-4, 37	4.9	Silt	0.26	0.13	10	127.87	3.25	0.0051
7R-5, 51	172.3	Sndst.	0.17	0.11	15	67.38	1.46	0.0029	1H-5, 36	6.3	Silt	0.33	0.11	5	131.38	2.73	0.0065
8R-4, 34	180.2	Siltst.	0.17	0.08	10	92.70	2.46	0.0035	1H-6, 24	7.7	Silt	0.99	0.11	10	130.76	2.76	0.006
9R-1, 95	186.1	Siltst.	0.07	0.03	10	71.10	1.80	0.0025	2H-1, 79	9.1	Silt	0.63	0.24	5	132.21	3.08	0.0062
9R-5, 84	191.9	Mxd. sed.	0.02	0.03	55	75.62	1.53	0.0029	2H-2, 72	10.5	Silt	0.63	0.22	5	126.45	2.90	0.0061
9R-6, 2	192.6	Mxd. sed.	0.03	0.01	7.5	67.73	1.53	0.0025	2H-3, 79	12.1	Silt	0.51	0.20	5	120.02	2.90	0.0057
10R-2, 22	196.4	Mxd. sed.	0.04	0.03	35	58.56	1.56	0.0024	2H-4, 79	13.6	Silt	0.45	0.19	5	120.18	2.69	0.006
11R-1, 114	205.5	Cgt.	0.16	0.11	15	104.21	3.00	0.0023	2H-5, 79	15.1	Silt	0.59	0.20	5	120.54	2.65	0.0055
13R-2, 62	225.8	Mxd. sed.	0.23	0.06	7.5	138.54	3.15	0.0036	2H-6, 79	16.6	Silt	0.99	0.20	17	115.72	2.85	0.0052
13R-3, 14	226.8	Mxd. sed.	0.13	0.07	12.5	125.12	3.03	0.0031	3H-2, 80	20.1	Silt	0.52	0.21	7	123.84	3.30	0.005
14R-2, 118	236	Siltst.	0.22	0.10	10	129.07	4.27	0.0032	3H-2, 117	20.5	Silt	0.41	0.17	7	125.38	3.34	0.0052
14R-3, 62	236.9	Siltst.	0.03	0.02	10	99.67	3.90	0.0022	3H-2, 134	20.6	Silt	0.37	0.13	5	162.29	3.25	0.0055
15R-3, 50	246.5	Cgt.	0.09	0.04	10	95.73	2.69	0.0026	3H-2, 144	20.7	Silt	0.42	0.13	5	141.78	3.20	0.0063
Hole 828A									3H-3, 78	21.6	Silt	0.46	0.19	5	131.51	3.07	0.0056
4H-1, 83	24.2	Silt	0.38	0.16	7.5	88.10	2.32	0.0035	3H-4, 53	22.8	Silt	0.43	0.20	10	147.53	3.46	0.0061
5H-4, 57	38	Silt	0.33	0.20	20	123.74	3.21	0.0044	3H-5, 66	24.5	Silt	1.11	0.19	5	154.41	3.96	0.0064
8H-1, 44	61.8	Ooze	0.09	0.01	3	17.04	0.56	0.0012	3H-6, 60	25.9	Silt	0.89	0.19	5	144.96	3.89	0.0058
8H-6, 69	69.6	Ooze	0.01	0.01	20	11.13	0.56	0.0005	3H-7, 22	27	Silt	0.97	0.16	15	151.98	4.09	0.0062
8H-7, 5	70.5	Ooze	0.03	0.01	2.5	12.51	0.57	0.0006	4H-1, 35	27.7	Silt	0.99	0.23	25	137.48	3.30	0.0058
9H-6, 89	79.3	Ooze	0.00	0.00	40	6.86	0.54	0.0002	4H-1, 119	28.5	Silt	0.68	0.05	5	127.44	3.15	0.0056
9H-7, 29	80.2	Ooze	0.02	0.01	5	7.65	0.47	0.0003	4H-2, 29	29.1	Silt	0.86	0.10	5	155.05	3.94	0.0068
10H-1, 116	81.6	Ooze	0.01	0.01	27.5	10.19	0.74	0.0004	4H-2, 105	29.9	Silt	1.30	0.19	5	123.08	3.17	0.0051
11H-1, 20	90.1	Ooze	0.01	0.01	15	13.65	0.65	0.0006	5H-1, 29	30.6	Silt	0.67	0.09	5	137.47	3.07	0.0058
11H-3, 126	94.2	Breccia	0.00	0.00	5	0.50	0.03	0.0001	5H-1, 120	31.5	Silt	0.59	0.11	5	136.70	3.05	0.0056
Hole 828B									5H-2, 31	32.1	Silt	0.61	0.14	5	127.51	3.21	0.0053
1R-2, 45	92	Chalk	0.03	0.01	40	5.68	0.34	0.0003	5H-2, 90	32.7	Silt	0.50	0.13	5	116.95	2.92	0.0048
1R-2, 98	92.5	Chalk	0.04	0.01	1	6.38	0.34	0.0003	5H-3, 66	34	Silt	0.48	0.10	5	121.78	3.07	0.0045
1R-4, 60	95.1	Chalk	0.04	0.02	15	13.85	0.44	0.0006	5H-4, 32	35.1	Silt	0.52	0.11	5	123.48	3.23	0.0047
Hole 829A									5H-4, 124	36	Silt	0.52	0.11	5	116.55	3.16	0.0044
5R-1, 9	31.1	Silt	0.89	0.14	30	149.80	3.99	0.0059	5H-5, 20	36.5	Silt	0.60	0.13	5	119.45	3.29	0.0046
5R-3, 85	34.9	Silt	0.68	0.18	5	122.50	4.26	0.0039	5H-5, 62	36.9	Silt	0.43	0.09	5	95.51	3.43	0.0028
7R-1, 30	51.1	Silt	0.29	0.06	2	93.39	2.26	0.0005	7H-1, 68	48.2	Mxd. sed.	0.30	0.06	5	66.18	1.58	0.0029
12R-1, 35	99.4	Chalk	0.05	0.03	10	35.62	0.92	0.0014	7H-1, 110	48.6	Mxd. sed.	0.33	0.07	5	69.73	1.68	0.0026
17R-1, 139	148.6	Silt	0.37	0.12	5	128.80	3.39	0.0046	7H-2, 32	49.3	Mxd. sed.	0.50	0.10	5	96.41	2.21	0.0031
17R-2, 70	149.4	Siltst.	0.36	0.13	5	144.99	4.02	0.0041	8H-1, 28	50.3	Silt	1.12	0.27	5	52.15	1.28	0.0025
17R-3, 88	151.1	Siltst.	0.19	0.11	12	86.41	2.82	0.0029	9H-1, 24	52.2	Silt	0.35	0.09	5	58.21	1.47	0.0022
17R-4, 23	151.9	Siltst.	0.23	0.04	5	82.71	2.84	0.0024	9H-3, 99	5.6	Ooze/silt	0.24	0.07	5	46.65	1.47	0.0017
17R-6, 19	154.9	Siltst.	0.42	0.13	5	122.95	2.96	0.0039	9H-4, 59	57.1	Ooze	0.11	0.03	5	18.13	0.53	0.0007
17R-6, 123	155.9	Siltst.	0.65	0.05	5	108.20	3.32	0.0051	Hole 830A								
17R-7, 28	156.5	Siltst.	0.40	0.26	12	90.64	3.78	0.0023	1H-1, 8	0.1	Silt	0.34	0.23	20	162.03	3.13	0.0033
18R-1, 107	157.9	Siltst.	0.21	0.08	5	117.02	3.05	0.0048	1H-1, 27	0.3	Silt	0.34	0.25	25	114.87	2.71	0.0032
18R-3, 76	160.6	Siltst.	0.10	0.03	8	105.42	3.59	0.0033	1H-1, 41	0.4	Silt	0.33	0.22	17	113.38	2.87	0.0033
18R-4, 28	161.6	Siltst.	0.35	0.24	15	130.39	3.23	0.0058	1H-1, 100	1	Silt	0.38	0.21	12	122.46	3.03	0.0038
18R-5, 107	163.9	Siltst.	0.26	0.15	10	115.83	2.87	0.0051	1H-2, 103	2.5	Silt	0.28	0.14	10	169.12	2.37	0.0038
18R-6, 30	164.6	Siltst.	0.15	0.09	15	87.46	2.31	0.0037	1H-3, 82	3.8	Silt	0.23	0.09	7	116.91	2.74	0.0041
19R-1, 73	167.2	Siltst.	0.48	0.14	5	73.89	3.53	0.0034	1H-4, 71	5.2	Silt	0.33	0.18	12	98.04	3.65	0.0022
19R-4, 37	171.4	Siltst.	1.26	0.16	10	117.49	2.55	0.008	1H-5, 40	6.4	Silt	0.27	0.12	7	99.61	2.22	0.0038
19R-5, 73	173.2	Breccia	0.93	0.11	4	81.70	2.21	0.0043	2H-1, 86	7.9	Silt	0.39	0.11	3	13.69	2.51	0.0042
20R-1, 116	177.3	Breccia	0.02	0.01	10	12.61	0.71	0.0003	2H-2, 63	9.1	Silt	0.60	0.08	3	111.12	1.76	0.006
20R-1, 135	177.5	Breccia	0.01	0.01	10	6.05	0.30	0.0001	2H-2, 100	9.5	Silt	0.44	0.15	3	154.18	2.67	0.0047
20R-3, 2	179.1	Siltst.	0.13	0.07	10	97.61	2.30	0.0052	2H-3, 83	10.8	Silt	0.52	0.23	7	115.68	2.90	0.0049
24R-1, 44	215.3	Breccia	0.05	0.03	15	24.87	0.94	0.0038	2H-5, 36	13.4	Silt	0.49	0.22	3	115.88	2.65	0.005
43R-1, 77	398.5	Chalk	0.01	0.01	10	28.55	0.99	0.0015	2H-6, 81	15.3	Silt	0.35	0.19	9	124.20	3.05	0.0036
43R-1, 144	399.2	Breccia	0.02	0.00	5	40.00	4.02	0.0014	2H-7, 51	16.5	Silt	0.57	0.24	7	115.35	2.54	0.0043
44R-2, 57	409.5	Chalk	0.16	0.08	15	70.19	1.33	0.0064	3H-1, 93	17.4	Silt	0.59	0.19	5	136.48	3.04	0.0051
51R-1, 23	460.3	Chalk	0.08	0.04	9	49.69	1.98	0.0019	3H-2, 47	18.5	Silt	0.33	0.11	5	121.85	2.77	0.005
51R-1, 108	461.2	Chalk	0.08	0.03	7	47.25	1.91	0.0018	3H-3, 60	20.1	Silt	0.02	0.01	5	5.62	0.16	0.0003
51R-2, 8	461.7	Chalk	0.07	0.03	8	40.66	1.49	0.0015	3H-3, 81	20.3	Silt						

Table 2 (continued).

Sample	Depth (mbsf)	Lithology	NRM (A/m)	RM ₁₀ (A/m)	MDF (mT)	IRM ₁₀₀₀ (A/m)	ARM ₁₀₀ (A/m)	K (SI)
3R-1, 18	67.9	Silt	0.57	0.26	7	146.71	3.71	0.0056
3R-1, 69	68.4	Silt	0.04	0.04	35	60.86	2.83	0.0014
3R-1, 98	68.7	Silt	0.01	0.01	20	26.41	1.22	0.0012
3R-1, 131	69	Silt	1.03	0.47	30	169.09	3.23	0.0079
4R-1, 15	77.7	Silt	0.49	0.35	20	143.22	3.38	0.005
4R-1, 83	78.3	Silt	0.44	0.34	20	126.54	2.99	0.0047
4R-2, 31	78.9	Silt	0.59	0.39	15	166.96	3.39	0.0077
5R-2, 51	89.4	Silt	0.52	0.33	15	147.22	3.19	0.0064
5R-2, 93	89.8	Silt	0.75	0.31	5	157.26	2.88	0.008
5R-2, 101	89.9	Silt	0.36	0.26	20	138.63	2.59	0.0063
6R-1, 20	97.3	Siltst.	0.43	0.32	20	170.32	4.33	0.007
6R-1, 81	97.9	Siltst.	0.38	0.22	12	150.56	3.10	0.0071
7R-1, 87	107.7	Siltst.	0.87	0.25	5	153.50	2.89	0.0087
8R-1, 119	117.7	Siltst.	0.52	0.34	15	186.87	6.37	0.0096
8R-2, 36	118.4	Siltst.	0.40	0.28	17	243.43	4.25	0.0148
9R-2, 44	128.1	Sandst.	0.78	0.21	5	144.60	2.68	0.0066
10R-2, 8	137.4	Sandst.	0.34	0.26	20	128.77	2.96	0.0047
12R-2, 49	157.3	Siltst.	0.15	0.05	7	152.98	2.91	0.0064
13R-1, 139	166.6	Siltst.	0.12	0.11	30	127.51	2.97	0.0044
15R-1, 41	185	Sandst.	0.18	0.05	5	86.93	2.15	0.0049
15R-1, 63	185.2	Sandst.	0.17	0.05	5	100.80	2.17	0.0054
15R-1, 107	185.7	Sandst.	0.63	0.04	5	65.94	2.68	0.0019
17R-1, 27	204.1	Silt	0.11	0.01	5	34.54	2.26	0.0009
18R-1, 39	213.8	Sandst.	0.12	0.02	5	225.84	8.01	0.0054
18R-1, 112	214.5	Breccia	0.04	0.03	20	136.57	4.08	0.0047
19R-1, 20	223.3	Sandst.	0.15	0.07	10	165.43	7.13	0.0048
19R-1, 100	224.1	Sandst.	0.21	0.02	5	93.27	5.30	0.0023
19R-1, 131	224.4	Sandst.	0.01	0.01	10	19.75	1.38	0.0007
19R-2, 15	224.8	Sandst.	0.01	0.00	5	6.21	0.33	0.0003
20R-1, 43	233.3	Sandst.	0.00	0.00	?	2.66	0.33	0.0001
20R-1, 93	238.3	Sandst.	0.00	0.00	10	3.86	0.46	0.0002
22R-1, 83	253.2	Sandst.	0.05	0.03	8	197.41	7.79	0.0053
23R-2, 44	264.1	Sandst.	0.01	0.01	40	68.38	1.65	0.0021
23R-2, 77	264.5	Sandst.	0.07	0.03	10	51.59	2.41	0.0021
24R-1, 60	272.6	Sandst.	0.05	0.03	30	207.38	5.68	0.0049
24R-1, 69	272.7	Sandst.	0.07	0.06	20	220.21	5.09	0.0102
Hole 830C								
1R-1, 71	235.7	Sandst.	0.11	0.03	5	154.95	3.60	0.0109
2R-1, 71	245.1	Sandst.	0.08	0.03	4	149.12	4.98	0.0038
2R-1, 116	245.6	Sandst.	0.89	0.09	5	452.45	9.03	0.0144
2R-1, 145	245.9	Sandst.	0.02	0.01	3	39.33	1.45	0.0017
4R-1, 123	264.9	Sandst.	0.08	0.04	11	84.03	4.05	0.0036
4R-2, 111	266.3	Breccia	0.15	0.02	5	39.00	1.83	0.0019
6R-1, 113	284	Breccia	0.50	0.14	5	267.43	7.18	0.0051
7R-1, 20	292.8	Sandst.	0.04	0.01	3	92.38	4.44	0.0031
7R-1, 66	293.3	Sandst.	0.06	0.01	5	118.73	6.71	0.0057
8R-1, 125	303.6	Sandst.	0.21	0.01	5	87.59	10.32	0.0023
8R-2, 5	303.9	Sandst.	0.07	0.02	6	71.47	3.77	0.0028
9R-1, 13	312	Sandst.	0.04	0.01	5	87.66	6.10	0.0026
9R-1, 26	312.2	Sandst.	0.04	0.02	5	74.14	4.47	0.0022
9R-1, 83	312.7	Sandst.	0.10	0.07	20	205.22	4.78	0.0092
10R-1, 15	321.7	Sandst.	1.16	0.08	15	212.68	5.13	0.0118
10R-2, 27	323.3	Sandst.	0.22	0.02	5	93.72	4.83	0.0034
12R-2, 64	343	Sandst.	0.49	0.13	5	160.33	2.24	0.0103
12R-2, 74	343.2	Sandst.	0.21	0.02	5	57.86	2.11	0.0019
12R-2, 111	343.5	Sandst.	0.19	0.11	7	209.43	9.15	0.0065

134 samples by AF demagnetization at a peak field of 10 mT. Hence, both NRM intensity and intensity remaining after 10-mT (RM₁₀) demagnetization are presented.

Ten well lithified mini-core samples of siltstone and sandstone from Sites 829 and 830 were thermally demagnetized using a Schonstedt thermal demagnetizer (Model TSD-1) aboard ship. Samples were heated at temperature intervals between 20°C and 50°C up to 500°C, and the remanence was measured between steps.

The manner in which isothermal remanent magnetization (IRM) and anhysteretic remanent magnetization (ARM) are acquired and demagnetized also provides information on the type of magnetic carriers and the coercivity spectrum of the sample. After AF demagnetization, the acquisition behavior of ARM was studied for a suite of 10 pilot samples. The Schonstedt AF demagnetizer and a DTECH double-coil anhysteretic magnetizer were used to produce the ARM. The alternating field was progressively increased from 0 to 100 mT in a DC-bias field of 0.1 mT. The ARM was then AF demagnetized so the demagnetization behavior could be compared to that of NRM and IRM. Subsequently, an ARM (ARM₁₀₀) was imparted to the 209 samples in the study using an alternating field of 100 mT and a DC-

bias field of 0.1 mT. The samples were then AF demagnetized at peak fields of 95 or 100 mT prior to giving the samples an IRM.

The IRM acquisition behavior of the pilot samples was studied at TAMU. Impulse fields increasing from 0 to approximately 1.0 T were applied along the -Z-axis of the sample using an ASC impulse magnetizer (Model IM-10). The remanence was measured between steps using the spinner magnetometer. The coercivity of saturation remanence (H_{CR}) of the samples was determined by applying an increasing reverse-field IRM (along the +Z-axis) to the samples. A second IRM was then applied (at a saturating field of about 1.0 T) and demagnetized using the Schonstedt AF demagnetizer so that the demagnetization behavior of IRM could be compared to that of NRM and ARM. An IRM was then applied to all samples in the study at a field of about 1.0 T (IRM₁₀₀₀).

Anisotropy of magnetic susceptibility of several samples from Hole 829A was measured by B. Ellwood at the University of Texas, Arlington, using a low-field torque magnetometer. All samples were taken near or within shear zones. Magnetic fabric is the three-dimensional variation of magnetic properties within a sample. This variation is determined by measuring the magnetic property in several different sample orientations, a procedure that reveals the anisotropy of magnetic properties in the sample. The magnitudes and directions of the property being measured define an ellipse, the shape of which provides information about the orientation of the magnetic minerals in the rock (Hrouda, 1982). This type of analysis is useful for determining orientation of foliation planes and degree of deformation (Hrouda, 1982). The samples were not corrected for orientation: most samples came from cores for which recovery was poor, so that structural and paleomagnetic corrections could not be made. Nevertheless, fabric information can be obtained from the shape of the ellipsoid.

Either ratios or differences among the principal axes (maximum, intermediate, and minimum) of the susceptibility ellipsoid may be used as a measure of ellipsoid shape. In the following equations, K_{MAX} is the maximum axis, K_{INT} is the intermediate axis, K_{MIN} is the minimum axis of the anisotropy ellipsoid, and K_{AVG} is $(K_{MAX} + K_{INT} + K_{MIN})/3$. The total anisotropy is defined by $(K_{MAX} - K_{MIN})/K_{AVG}$. The degree of anisotropy, P , is defined as the ratio K_{MAX}/K_{MIN} and describes the amount of preferred orientation of magnetic minerals in the sample. The q factor, defined as $(K_{MAX} - K_{INT})/(K_{MAX} + K_{INT})/2 - (K_{MIN})/K_{AVG}$, is used to measure the shape of the ellipsoid in sediments. For most sedimentary rocks, q ranges from about 0.06 to 0.67 (Tarlinton, 1983, and references therein). Increases in deformation of sediment in rocks whose degree of anisotropy (P) is less than about 1.05 have been correlated with increases in q (Hrouda, 1982). Magnetic lineation (L) is $(K_{MAX} - K_{INT})/K_{AVG} \times 100\%$, and measures the degree to which magnetic minerals parallel each other in a linear fashion, defining a prolate anisotropy ellipsoid. Magnetic foliation (F) is $(K_{INT} - K_{MIN})/K_{AVG} \times 100\%$, and determines the degree of planar parallelism of magnetic minerals, which describe an oblate anisotropy ellipsoid.

RESULTS

Hysteresis

Hysteresis data from samples from Sites 827 through 829 are presented in Table 3 and Figure 3. The M_{RS}/M_S values all fall near the boundary between pseudo-single-domain and multidomain behavior. The shapes of Figures 3A, 3C, and 3D are typical of samples dominated by magnetite, whereas the shape of Figure 3B may result from a mixture of magnetite and hematite.

Susceptibility

The variation of susceptibility determined using the shipboard multisensor track with depth and lithologic type in Holes 827B, 828A, 829A, 830A, and 830B is illustrated and described in the appropriate site chapters of the *Initial Reports* volume (Collot, Greene, Stokking, et al., 1992) and in two chapters by Roperch et al. (this volume).

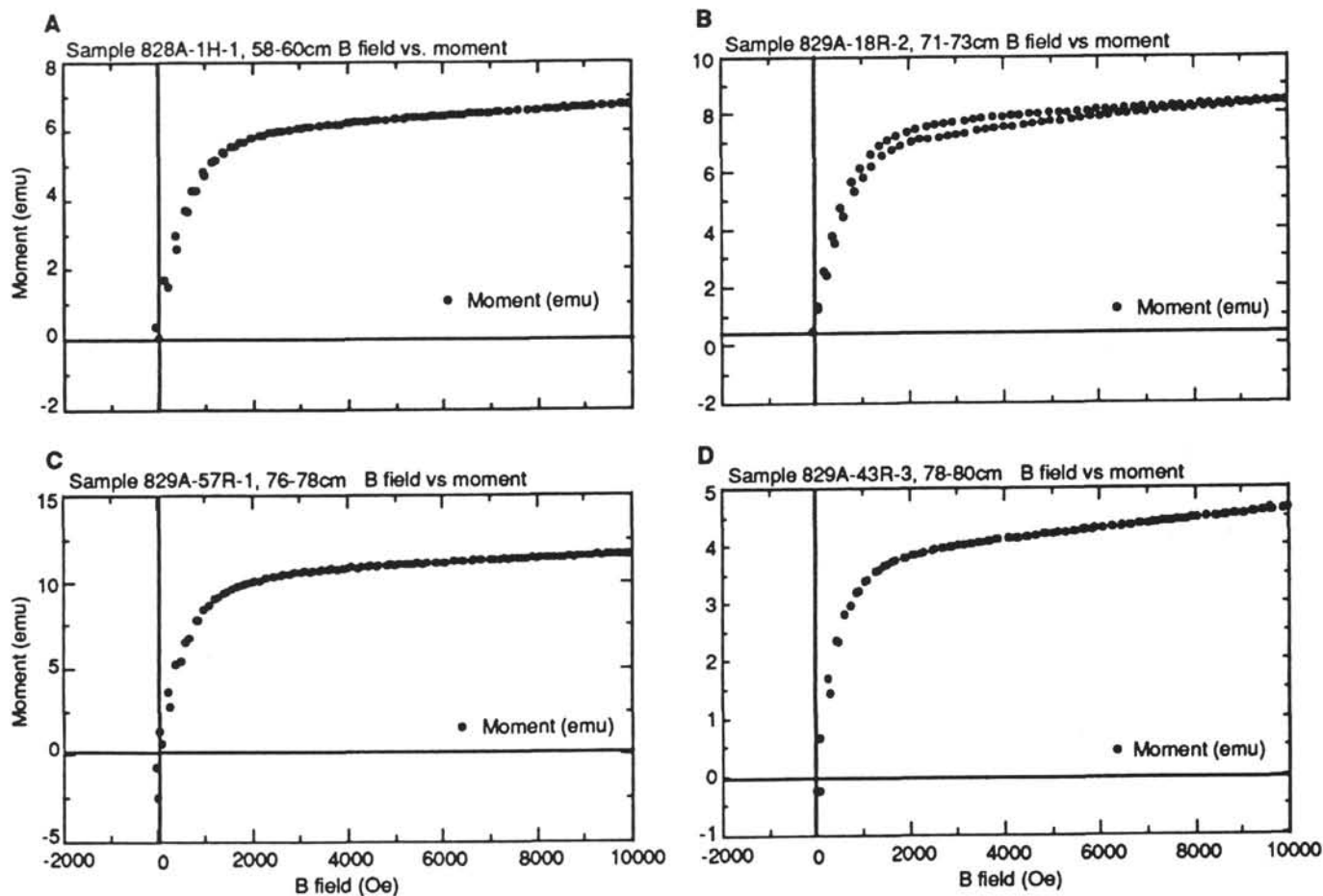


Figure 3. Hysteresis loops of representative samples. A. Sample 134-828A-1H-1, 58–60 cm. B. Sample 134-829A-18R-2, 71–73 cm. C. Sample 134-829A-57R-1, 76–78 cm. D. Sample 134-829A-43R-3, 78–80 cm.

Table 3. Hysteresis parameters.

Sample	Lith.	M_{RS}/M_S	B_{CR} (mT)	IRM_{1000} (A/m)
134-				
827A-9H-1, 24–27 cm	1	0.18	37	79.8
827A-12H-3, 73–75 cm	1	0.14	27	102.6
828A-1H-1, 58–60 cm	1	0.18	27	112.7
828A-3H-1, 62–64 cm	1	0.22	27	110.0
829A-4R-3, 98–101 cm	2	0.16	30	103.2
829A-18R-2, 71–73 cm	2	0.12	27	111.8
829A-43R-3, 78–80 cm	3	0.13	15	91.2
829A-51R-3, 24–26 cm	4	0.19	21	83.0
829A-57R-1, 76–86 cm	4	0.10	21	83.3
1. Volcanic silt				
2. Volcanic siltstone				
3. Ig-lithic breccia				
4. Volcanic sandstone				

Note: Lith. = lithology, M_{RS}/M_S = saturation remanent magnetization/saturation magnetization, B_{CR} = coercivity of remanence, IRM_{1000} = isothermal remanent magnetization at 1.0 T applied field.

Volume magnetic susceptibility of discrete samples of silt and siltstone ranges from 0.0002 to 0.0249 SI, with an average of 0.0056 SI. The susceptibility of sand and sandstone averages 0.0052 SI and varies from 0.0001 to 0.0173 SI, whereas that of breccias and conglomerates averaging 0.0022 SI ranges from 0.0001 to 0.0051 SI. Susceptibility of discrete samples of calcareous oozes and chalks averages 0.0013 SI and ranges from 0.0007 to 0.0064 SI, and that of mixed sediment samples varies from 0.0024 to 0.0036 SI with an

average of 0.0029 SI (Table 2). The downhole variation of magnetic susceptibility in Holes 827B, 829A, 829C, 830A, and 830B is illustrated in Figure 4.

NRM

Intensity of NRM ranges from 0.010 to 1.964 A/m (average 0.52 A/m) in the silts and siltstones, from 0.12 to 1.794 A/m (average 0.16 A/m) in the sands and sandstones, from 0.0005 to 0.93 A/m in the breccias and conglomerates, from 0.003 to 0.24 A/m (average 0.06 A/m) in the calcareous oozes and chalks, and from 0.02 to 0.50 A/m (0.20 A/m) in mixed sediment (Table 2). The NRM of all samples in this study most probably includes a depositional remanence (DRM), possibly a post-depositional remanence (pDRM), and a drilling-induced remanence.

Demagnetization Behavior

Remanent intensity after AF demagnetization at 10 mT (RM_{10}) varies from 0.003 to 0.471 A/m (average 0.16 A/m) in the silts and siltstones, from 0.001 to 0.366 A/m (average 0.04 A/m) in the sands and sandstones, from 0.0005 to 0.14 A/m (average 0.06 A/m) in the breccias and conglomerates, from 0.005 to 0.083 A/m in the calcareous oozes and chalks, and from 0.014 to 0.102 A/m (average 0.06 A/m) in mixed sediment (Table 2). Vector endpoint diagrams illustrating the AF demagnetization behavior of samples from the pilot study are presented in Figure 5. The steep, negative, drilling-induced component is evident in all samples and is significantly reduced by

demagnetization at 10 mT. The downhole variation of RM_{10} in Holes 827B, 829A, 829C, 830A, and 830B is illustrated in Figure 6.

The median destructive field (MDF) is the peak demagnetizing field at which half the NRM has been removed. MDF values for samples in this study are provided in Table 2. Although these data provide information about the relative coercivities of the samples, the values should be interpreted with caution because of the drilling-induced component of the NRM. Nevertheless, the remanence of most samples is demagnetized at relatively low peak fields, consistent with the dominant carrier of remanence being titanomagnetite, with a relatively large multidomain component.

The results of thermal demagnetization of samples of well lithified siltstone from Core 134-829A-56R are illustrated in Figure 7. The remanence of all samples measured was unblocked by heating at temperatures between 450°C and 500°C, consistent with either titanomagnetite, magnetite, or hematite as the carrier of remanence.

Laboratory-induced Remanences

Figures 8 and 9 illustrate IRM and ARM acquisition behavior and remanence decay after AF demagnetization of typical samples from the pilot study. The shapes of the acquisition curves are typical of titanomagnetite. The IRM acquisition curves rise sharply, then flatten, indicating that little, if any, hematite is present. In most samples, saturation is achieved at an impulse field of approximately 0.1 T.

IRM_{1000} ranges from 5.62 to 243.4 A/m (average 125.58 A/m) in silts and siltstones, from 2.66 to 452.4 A/m (average 121.65 A/m) in the sands and sandstones, from 0.50 to 267.4 A/m (average 68.27 A/m) in the breccias and conglomerates, from 5.68 to 70.19 A/m (average 25.11 A/m) in the calcareous oozes and chinks, and from 58.56 to 138.5 A/m (average 87.24 A/m) in mixed sediment (Table 2). Especially in the silts, siltstones, sands, and sandstones, IRM_{1000} intensities are quite high, reflecting the abundance of titanomagnetite in the samples. ARM_{100} ranges from 0.16 to 6.37 A/m (average 3.05 A/m) in silts and siltstones, from 0.33 to 10.32 A/m (average 3.97 A/m) in the sands and sandstones, from 0.03 to 7.18 A/m (average 2.26 A/m) in the breccias and conglomerates, from 0.34 to 1.98 A/m (average 0.89 A/m) in the calcareous oozes and chinks, and from 1.53 to 3.15 A/m (average 2.03 A/m) in mixed sediment (Table 2). The ARM_{100} and IRM_{1000} of the pilot samples were demagnetized so that the stability of ARM and IRM could be compared to that of NRM.

Magnetic Fabric

Results of measurements of anisotropy of magnetic susceptibility from deformed intervals in Hole 829A are listed in Table 4, and a comparison of lineation and foliation is presented in Figure 10. Plate 2 contains photomicrographs of samples of breccia (Sample 134-829A-43R-1, 144–146 cm) and brown clay (Sample 134-829A-47R-1, 57–59 cm) from shear zones.

DISCUSSION

Magnetic Mineralogy

Preliminary scanning electron and energy-dispersive x-ray microanalyses of magnetic mineral separates from typical samples of volcanic silt from Holes 827A and 829A are illustrated in Plate 3. SEM and qualitative X-ray analysis indicate that titanomagnetite, relatively low in titanium, is the dominant carrier of remanence (Pls. 2 and 3). The shapes of the IRM and ARM acquisition curves and the behavior during AF and thermal demagnetization are consistent with titanomagnetite as the predominant magnetic mineral.

Particle Size

Rock magnetic data can be used to constrain the size of magnetic particles in the samples. For equidimensional grains, pure magnetite

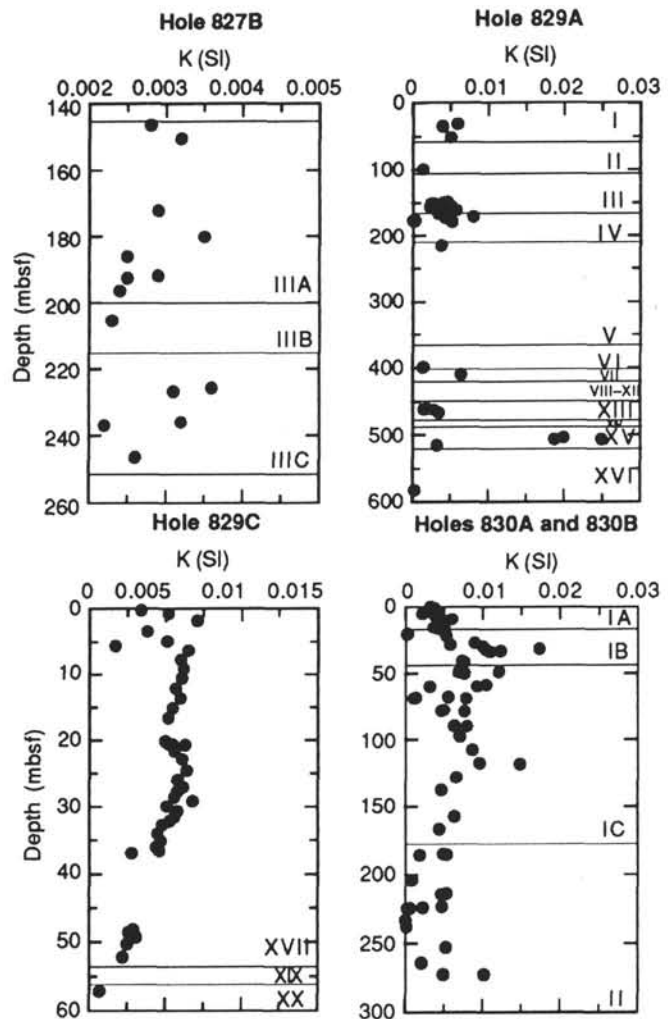


Figure 4. Downhole variation of magnetic susceptibility (K) in Holes 827B, 829A, 829C, 830A, and 830B.

is superparamagnetic when less than about 0.03 μm in diameter, single domain from 0.03 to 0.08 μm in diameter, and typically exhibits multidomain at diameters greater than 0.2 μm (Butler and Banerjee, 1975). Particles larger than typical single-domain grains that show single-domain behavior are considered pseudo-single domain. The diameters at which transitions between stable domain states occur depend upon the composition of the particle, however, and vary with the concentration of cations in solid solution with Fe, particularly Ti, but also Al, Mg, and Mn. Considering only the influence of Ti, titanomagnetite containing 60% ulvospinel (Fe_2TiO_4) does not show single domain behavior until its diameter has increased to 0.08 μm (Dunlop, 1981); the transition from single domain to multidomain behavior theoretically should occur at 0.2 μm (Butler and Banerjee, 1975) and has been observed to occur at about 0.6 μm (Soffel, 1971). In addition, domain behavior is affected by the elongation of the particle (Butler and Banerjee, 1975), the structure of the grain, oxidation, or microcracks (Haggerty, 1970; Johnson and Hall, 1978; Henshaw and Merrill, 1980) that may produce regions within a large grain that act as single domains.

The ratio of hysteresis parameters M_{RS}/M_S has been used to distinguish between single-domain and multidomain behaviors: values greater than 0.5 indicate single-domain particles, ratios between about 0.1 and 0.5 represent pseudo-single domain particles, and values less than about 0.1 indicate multidomain or superparamagnetic particles (Stoner and Wohlfarth, 1948; Day et al., 1977; Thompson and Oldfield,

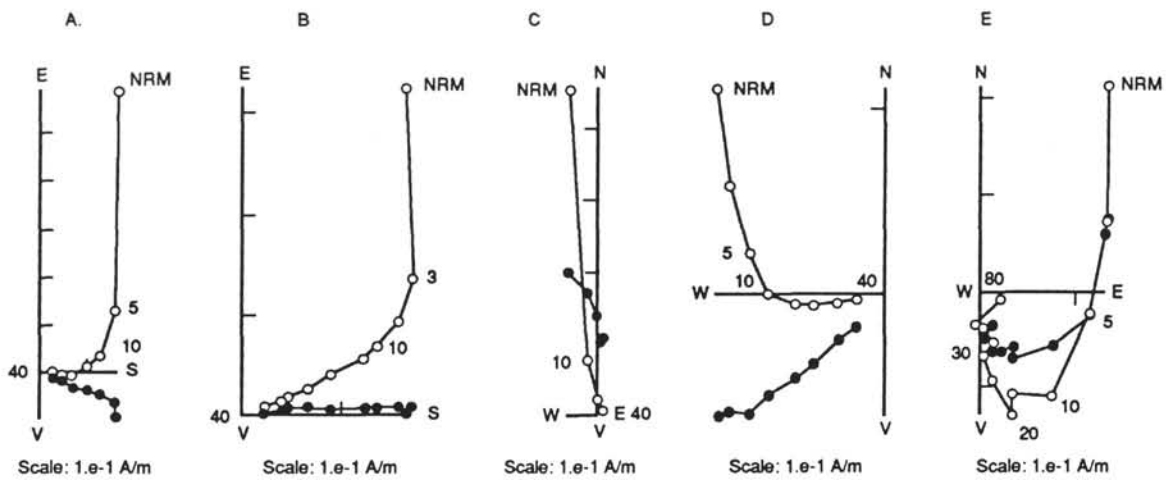


Figure 5. Vector endpoint diagrams illustrating the results of AF demagnetization of NRM of representative samples. Solid circles represent the horizontal component of remanence and open circles represent the vertical component. NRM, RM_{10} , final, and some additional peak demagnetizing fields (mT) are indicated. **A.** Volcanic silt (Sample 134-829C-5H-2, 31 cm). **B.** Volcanic siltstone (Sample 134-829A-17R-2, 70 cm). **C.** Breccia (Sample 134-830C-6R-1, 113 cm). **D.** Chalk (Sample 134-829A-44R-2, 57 cm). **E.** Mixed sediment (Sample 134-827B-9R-6, 2 cm).

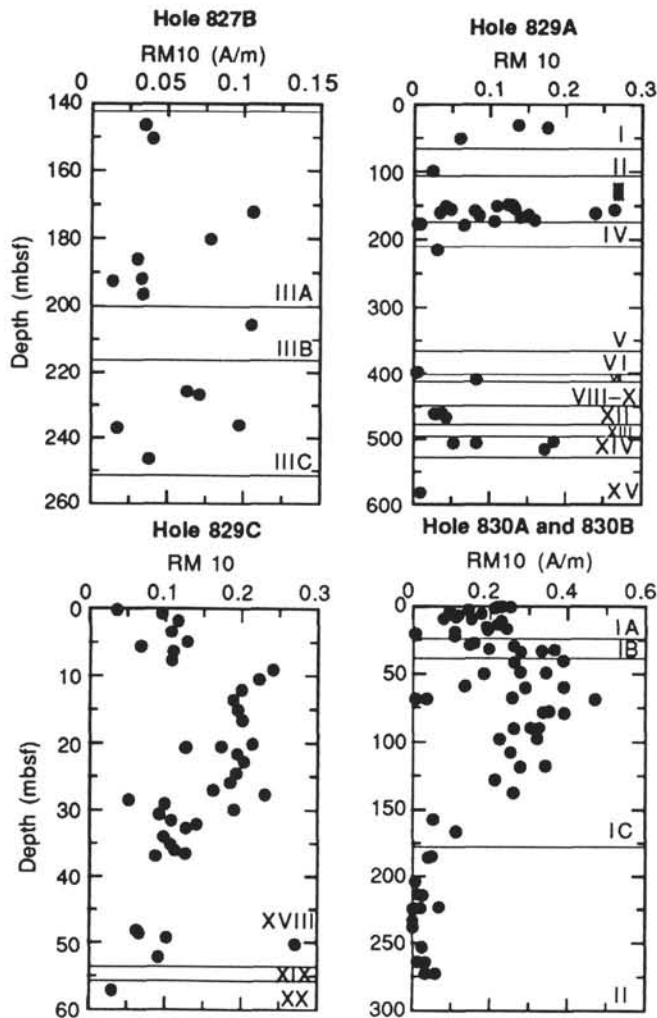


Figure 6. Downhole variation of RM_{10} in Holes 827B, 829A, 829C, and 830A and 830B.

Table 4. Anisotropy data. Acronyms and abbreviations are defined in the text.

Sample	Depth (mbsf)	<i>P</i>	<i>q</i>	<i>F</i> (%)	<i>L</i> (%)	Aniso. (%)
134-829A-						
12R-1, 24	99.24	1.01	0.76	0.55	0.68	1.23
12R-1, 55	99.55	1.06	0.61	3.32	2.93	6.24
43R-1, 20	397.27	1.11	0.85	4.36	6.43	10.79
43R-1, 139	399.09	1.04	0.61	2.07	1.79	3.86
43R-2, 27	399.47	1.06	0.87	2.24	3.42	5.66
43R-2, 69	399.89	1.05	1.26	1.04	3.52	4.56
47R-1, 51	427.11	1.04	0.59	2.19	1.82	4.01
47R-1, 57	427.17	1.08	0.63	4.12	3.75	7.87
51R-1, 8	460.18	1.06	0.44	3.34	1.91	5.3
51R-1, 59	460.69	1.06	0.19	4.61	0.98	5.59
51R-2, 130	462.90	1.05	0.57	2.73	2.2	4.92
58R-1, 132	524.52	1.22	0.38	13.2	6.11	19.27

Note: Aniso. = total anisotropy.

1986). Although domain state is not a direct measure of particle size, the ratios may provide some indication of relative changes in domain behavior that reflect changes in particle size. Thus, on the basis of hysteresis parameters, the samples analyzed in this study fall near the boundary between pseudo-single domain and multidomain behavior.

Differences in the stabilities to AF demagnetization of natural and artificial remanences carried by magnetite are governed by particle size, the relative proportions of low- and high-coercivity particles, the degree of particle alignment, and the interplay between internal stresses within a particle and magnetostatic interactions between pinned and unpinned domain walls (Heider et al., 1992; Moon and Merrill, 1986; Stacey and Banerjee, 1974; Xu and Merrill, 1990; Xu and Dunlop, 1993). Lowrie and Fuller (1971) demonstrated that the relative stabilities to AF demagnetization of IRM and thermoremanent magnetization (TRM) may be used to evaluate the domain state that predominates in the primary carrier of remanence in a sample, assuming that the primary magnetization is carried by magnetite. For single-domain particles, TRM is more stable than IRM, whereas for multidomain particles, IRM is more stable than TRM. The stability of ARM to AF demagnetization is similar to that of TRM (Johnson et al., 1975; Levi and Merrill, 1976), which enabled the Lowrie-Fuller test to be modified to compare stabilities of ARM and IRM, thereby avoiding problems associated with mineralogical changes caused by heating the samples.

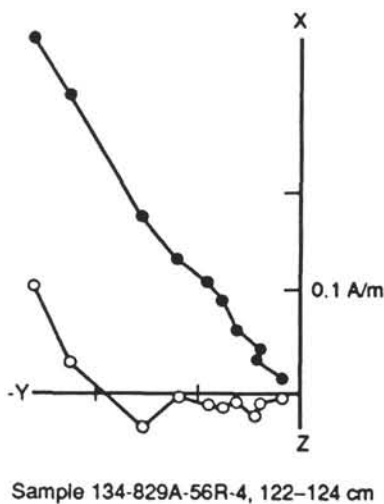
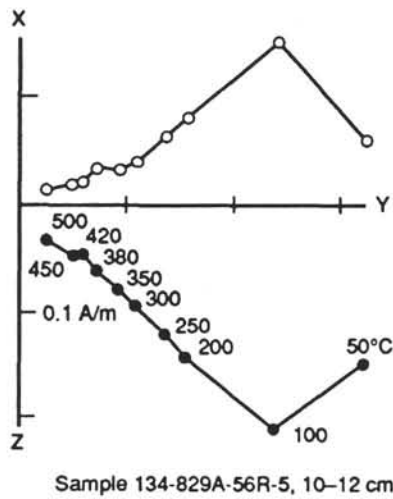


Figure 7. Thermal demagnetization behavior of volcanic siltstone samples from Hole 829A. Symbols as in Figure 5, temperature steps in $^{\circ}\text{C}$.

The validity of ARM as an analog to TRM may, however, depend on the concentration of the magnetic material (Sugiura, 1979).

Recent studies question interpretations of the Lowrie-Fuller test: the stability of multidomain particles depends on an interplay between the internal stresses that act to pin domain walls and a screening effect in which magnetostatic interactions between unpinned and pinned domain walls increases the particle's resistance to AF demagnetization (Moon and Merrill, 1986; Xu and Merrill, 1990; Heider et al., 1992; Xu and Dunlop, 1993). In grains with high internal stress, such as the crushed magnetite particles used by Lowrie and Fuller (1971), the effect of screening is small, and stability to AF demagnetization depends mostly on microcoercivity, and hence, particle size. Stability to AF demagnetization of particles whose internal stress is low, however, is controlled by screening, and thus shows less size dependence (Xu and Dunlop, 1993).

Experiments in which the Lowrie-Fuller test was modified by substituting ARM for TRM were not designed to simulate DRM, and did not take into account the effects of concentration or particle alignment on stability against AF demagnetization. Nonetheless, the modified Lowrie-Fuller test has been applied to marine sediments. Lowrie-Fuller test results were consistent with particle sizes determined using transmission electron microscopy when the test was applied to deep-sea sediments that contained single-domain biogenic and multi-

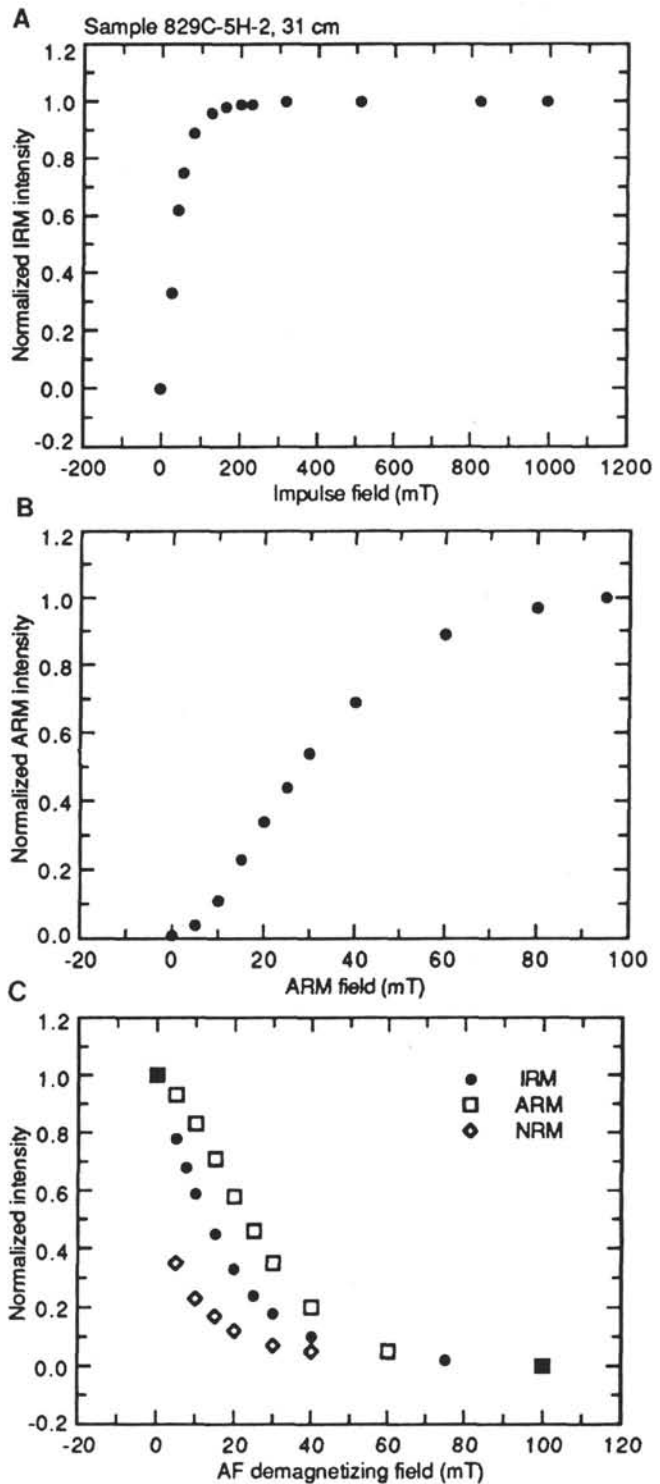


Figure 8. Rock magnetic behavior of volcanic silt (Sample 134-829C-5H-2, 31 cm). A. IRM acquisition. B. ARM acquisition. C. Intensity decay, AF demagnetization of NRM, IRM_{1000} , and ARM_{100} .

domain lithogenic magnetite (Petersen et al., 1986) and to carbonates that contained single-domain biogenic magnetite (McNeill, 1990). Apparent particle sizes indicated by the hysteresis parameters differed from those implied by the Lowrie-Fuller test, however, for suboxic sediments that probably contained magnetite from a variety of sources (Karlin, 1990). The test is probably most useful in sediments that

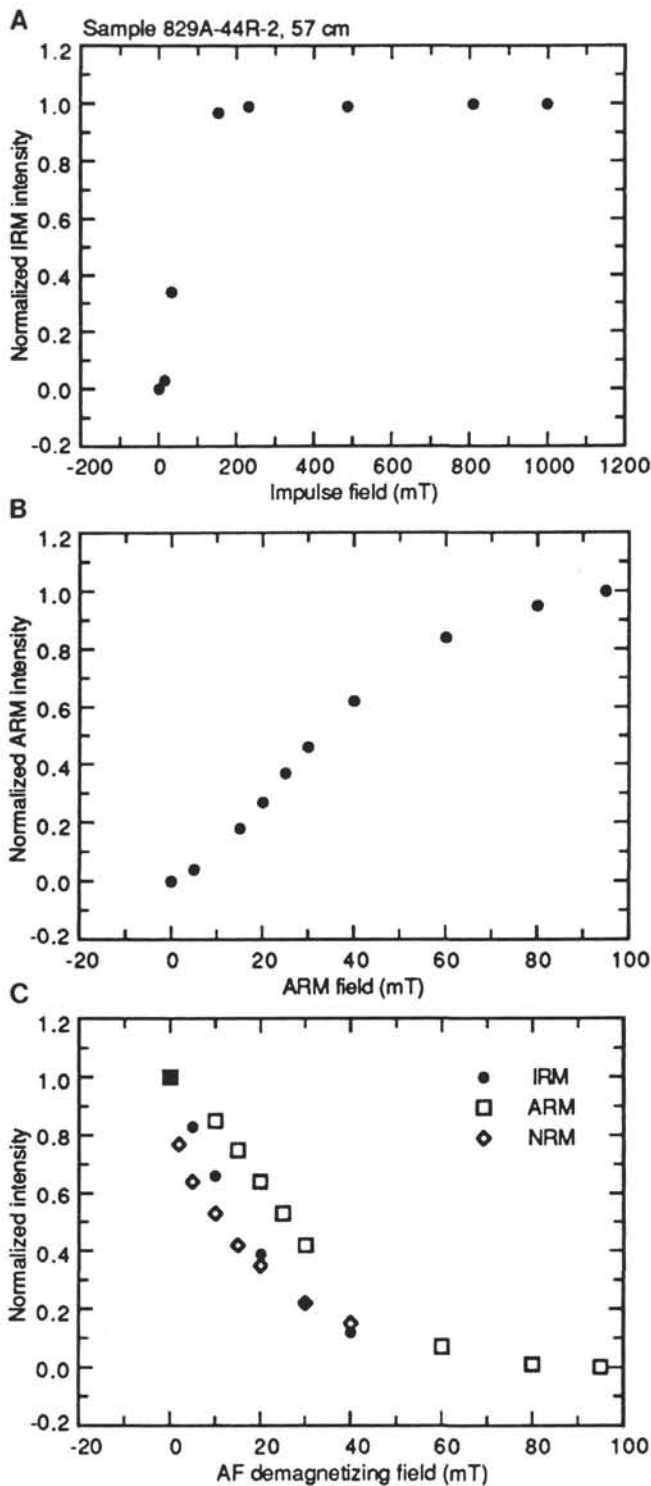


Figure 9. Rock magnetic behavior of chalk (Sample 134-829A-44R-2, 57 cm). A. IRM acquisition. B. ARM acquisition. C. Intensity decay, AF demagnetization of NRM, IRM₁₀₀₀, and ARM₁₀₀.

contain uniformly stressed magnetic particles whose stability is governed by microcoercivity rather than screening, and in which magnetostatic interactions between aligned particles are not significant.

In most Leg 134 samples, the stabilities of IRM and ARM to AF demagnetization are similar: ARM is slightly more stable to AF demagnetization than IRM, and both are much more stable than the NRM (Figs. 8C and 9C). A simple application of the Lowrie-Fuller test to

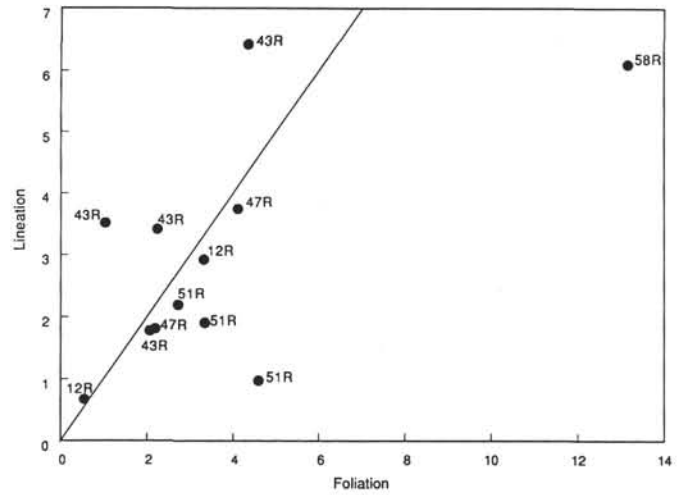


Figure 10. Hole 829A. Lineation vs. foliation.

these results would suggest that the samples contain single-domain material. Alternatively, the samples may contain multidomain particles whose stability against AF demagnetization is increased by magnetic screening or particles with a wide range of internal stresses. Considering that hysteresis data implied the presence of multidomain material, the samples may well contain mixtures of particle sizes and domain states.

Ratios of IRM₁₀₀₀ (or ARM₁₀₀) to susceptibility reflect changes in grain size of magnetic particles (Banerjee et al., 1981; King et al., 1982; Bloemendal et al., 1989; Sager and Hall, 1990). Figure 11 shows the downhole variation of IRM₁₀₀₀/K and Figure 12 is a plot of log K vs. log IRM₁₀₀₀. Susceptibility reflects the concentration of magnetic minerals, whereas IRM₁₀₀₀ and ARM₁₀₀ are controlled both by the concentration and particle size of magnetic minerals. If grain size is the same, susceptibility can be used to normalize out concentration variations. In Figures 11 and 12, a large proportion of fine-grained particles results in high ratios, whereas a preponderance of coarse-grained particles produces low ratios. The presence of superparamagnetic material will increase susceptibility, resulting in low ratios that do not reflect the presence of coarse-grained material (Thompson and Oldfield, 1986). This tests elucidates relative changes in particle size that correspond to sedimentological differences discussed below.

Correlation between Magnetic Properties and Lithostratigraphy

Figure 4 shows the downhole variation of magnetic susceptibility measured in discrete samples from Holes 827B, 829A, 829C, and 830A and 830B. Susceptibility peaks in all plots correspond to intervals of volcanic silt, siltstone, sand, and sandstone, and thus indicate increases in the contribution of volcanogenic material, either derived by erosion of arc rocks or from a volcanic eruption. Oozes, chalks, and calcareous breccias are marked by low susceptibilities. Intensities of NRM and RM₁₀ (Collot, Greene, Stokking, et al., 1992; and Figure 6) also reflect the abundance of titanomagnetite. Both display trends similar to the susceptibility.

In Hole 827B, Unit III contains highly bioturbated, partially lithified calcareous volcanic siltstone with intervals of conglomerate. Increases in susceptibility and intensity of remanence (Figs. 4 and 6) correspond to decreases in carbonate percentage (Collot, Greene, Stokking, et al., 1992). The IRM₁₀₀₀/K ratio increases in Subunits IIIA and IIIC, suggesting a fining upward of the relatively dense titanomagnetite grains which was not observed in sedimentological descriptions of the cores.

Units in Hole 829A that contain abundant volcanogenic minerals are characterized by high magnetic susceptibilities and intensities, as

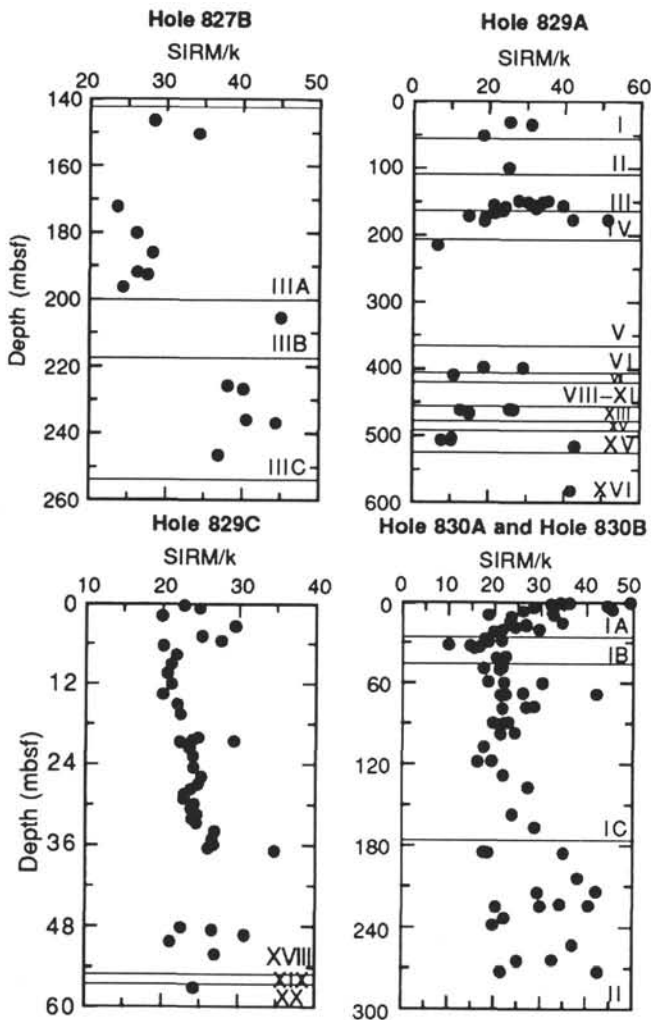


Figure 11. Downhole variation of IRM_{1000}/K in Holes 827B, 829A, 829C, and 830A and 830B.

expected. In Unit III, interbeds of volcanic sand are common, and an increase in grain size in the lower 15 m of the unit is reflected by a decrease in IRM_{1000}/K . Differences in magnetic susceptibility and intensity in Unit XIII, a volcanic sandstone, reflect differences in the amount of carbonate: intervals low in carbonate correspond to high magnetic susceptibility and intensity. Unit XV, a partially lithified sandy volcanic siltstone with chalk clasts, displays a wide range of susceptibility and intensity values as well as varying IRM_{1000}/K ratios.

Cores from Hole 829C are described as structureless clayey sandy volcanic silt with some poorly defined ash layers (Collot, Greene, Stokking, et al., 1992). Trends in magnetic susceptibility and intensity are similar: both suggest a gradational variation in the contribution of volcanogenic material. Peaks correspond to intervals described as containing ash layers. IRM_{1000}/K ratios tend to increase downhole, which corresponds to the observed decrease in grain size from clayey sandy volcanic silt to clayey volcanic silt (Collot, Greene, Stokking, et al., 1992). Lower IRM_{1000}/K ratios near the top of Unit XVIII in Hole 829C correspond to clay-rich intervals; higher ratios near the base of the unit reflect increases in the amount of sand. Fluctuations in the IRM_{1000}/K ratio reflect the variable amounts of clay and sand reported by shipboard sedimentologists.

Two major lithostratigraphic units were defined and described at Site 830 (Collot, Greene, Stokking, et al., 1992; Table 1). Lithostratigraphic Unit I is a dark-gray volcanic silt and siltstone that is subdivided into three subunits based primarily on the presence and

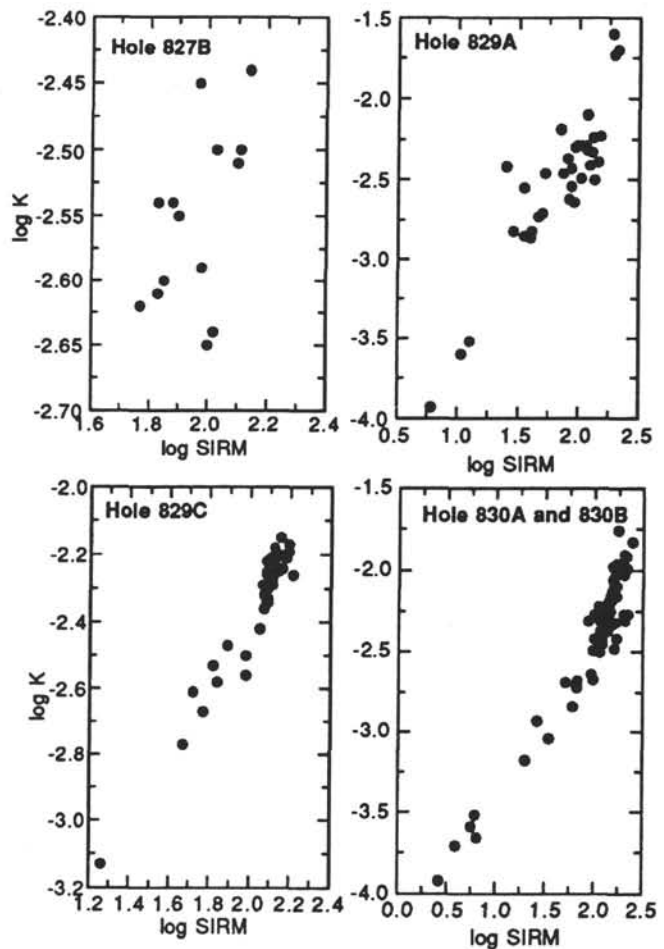


Figure 12. $\log K$ vs. $\log IRM_{1000}$.

character of sandy interbeds. Subunit IA consists of nearly structureless unlithified silt and contains ash layers 1 to 5 cm thick. Carbonate is more abundant in the upper part of the subunit. The decrease in carbonate downhole is reflected by an increase in magnetic susceptibility and intensity. A decrease in IRM_{1000}/K near the base of Subunit IA corresponds to an increase in the frequency of sandy layers. Subunit IB is clayey sandy silt with several normally graded interbeds of black sand and an increased proportion of volcanogenic minerals, notably plagioclase, clinopyroxene and opaque minerals. Subunit IC is a sequence of interbedded sandy silt and sand that contains less clinopyroxene and opaque minerals than Subunit IB. Variations in IRM_{1000}/K also reflect grading observed in Subunits IB and IC. An increase in the contribution of volcanogenic sediment is reflected by an increase in magnetic susceptibility and intensity in Subunit IB. Unit II comprises partially lithified, very poorly sorted, very coarse, volcanoclastic, silty sandstones. The sand grains in the sandstone are particles of well-lithified volcanic siltstone. The substantial scatter in all rock magnetic properties from Unit II samples results from the wide range of particle sizes observed in the unit.

Samples from Hole 829A define a fairly linear trend in a plot of $\log K$ vs. $\log IRM_{1000}$, although some scatter is apparent. Samples from Holes 829C and 830A and B lie along linear trends in $\log K$ vs. $\log IRM_{1000}$ plots.

Fabric: AMS and SEM Observations

Anisotropy parameters listed in Table 4 vary widely, even between very closely spaced samples. Figure 10 is a plot of lineation (L) vs. foliation (F). The straight line drawn on the plot indicates a slope of

unity and forms the boundary between ellipsoids that are predominantly prolate and those that are oblate (Hrouda, 1982). The magnetic fabric of Samples 134-829A-12R-1, 24 cm, -43R-2, 27 cm, and -43R-2, 69 cm, is thus prolate and dominated by lineation, whereas that of the remaining samples is oblate, and dominated by foliation, as is the structural fabric (Meschede and Pelletier, this volume). Scatter of anisotropy parameters was also observed in sediments from above the décollement in the Nankai Trough, and was attributed to strain inhomogeneity; below the décollement at Nankai, magnetic fabric was predominantly oblate (Owens, 1993).

Even in intensely deformed sediments, SEM observations reveal regions within individual beds in which deformation and parallel orientation of clay particles is not as apparent at high magnifications (e.g., 2000X) as it is at low magnifications (<100X). Sample 134-829A-43R-1, 144-146 cm, illustrated in Plate 2A and 2B, exhibits macroscopic folds and crenulations at magnifications of 100x. Investigation of the regions between folds at higher magnifications, however, reveals relatively little deformation. Plate 2B is a photomicrograph of a region within the sample in which platy minerals appear to parallel the bedding plane that forms the right flank of the fold pictured in the upper right corner of Plate 2A. Within a few micrometers of the bedding plane, however, this foliation becomes much less apparent, and grains appear to be more randomly oriented. Sample 134-829A-47R-1, 57-59 cm, was taken from a brown clay that, macroscopically, is intensely deformed and comprises a shear zone. Even at low magnifications, alignment of minerals is not apparent, although the degree of magnetic anisotropy, foliation, and lineation are rather high. These observations suggest that much of the deformation in the shear zones is accomplished by motion along bedding planes, whereas the intervals between these sheared planes retain some structural integrity.

In the brown clay of Core 134-829A-47R, foliation dominates the magnetic fabric. This trend continues in Cores 134-829A-51R and -58R, and similar oblate fabrics were observed in scaly clay zones at Barbados (Hounslow, 1990). No distinctions can be made about the relative importance of foliation and lineation in Cores 134-829A-12R and -43R. The variability of degree of anisotropy, P , and shape parameter, q , reflect the patchy nature of deformation in this hole.

CONCLUSIONS

1. The dominant carrier of remanence in the highly magnetic volcanogenic sediments and sedimentary rocks in the DEZ is low-titanium titanomagnetite of variable particle size, hence domain state.

2. Variation in magnetic property correlate to sedimentological changes. Changes in rock magnetic properties clearly reflect variations in the abundance and size of titanomagnetite particles, which in turn are linked to differences in lithologic type, and percentage of carbonate contents. In some cases, grain-size variations indicated by rock magnetic properties may show the presence of fining upward sequences and changes in amounts of volcanogenic material that are missed during visual core descriptions.

3. Although the AMS results are difficult to interpret in terms of regional stresses because the cores were unoriented, the variability of degree of anisotropy (P) and the shape parameter (q) reflect the patchy nature of deformation, at a micrometer scale, elucidated by SEM analysis. The magnetic fabric of sediment from Hole 829A shows that deformation in the shear zones is accomplished by motion along bedding planes, whereas the sediment within the beds themselves remains relatively undeformed. This corresponds to structural observations of the cores (Meschede and Pelletier, this volume).

ACKNOWLEDGMENTS

We thank J. Aguiar for assistance with data processing and presentation. W. Sager provided the use of his susceptibility meter, and J. Talese assisted with susceptibility and ARM measurements. We are grateful to J. Leonard for helpful comments and assistance and for

providing additional samples for SEM analysis. We thank K. Verosub for permitting us to use the vibrating sample magnetometer in the Physics Department at the University of California, Davis, and we are indebted to M. Sweitzer for her assistance with hysteresis measurements. We thank M. Meschede for allowing us to borrow shear-zone samples that he collected, the AMS of which were kindly measured by B. Ellwood at the University of Texas, Arlington. J. Gee and R. Musgrave provided valuable criticisms and advice. M. Hitchcox assisted with the preparation of the final manuscript. This research was supported by a grant to L. Stokking from the U.S. Science Support Program of the Joint Oceanographic Institutions, Inc.

REFERENCES*

- Banerjee, S.K., King, J., and Marvin, J., 1981. A rapid method for magnetic granulometry with applications to environmental studies. *Geophys. Res. Lett.*, 8:333-336.
- Bloemendal, J., King, J.W., Tauxe, L., and Valet, J.-P., 1989. Rock-magnetic stratigraphy of Leg 108 Sites 658, 659, 661, and 665, eastern tropical Atlantic. In Ruddiman, W., Sarnthein, M., et al., *Proc. ODP, Sci. Results*, 108: College Station, TX (Ocean Drilling Program), 415-428.
- Butler, R.F., and Banerjee, S.K., 1975. Theoretical single-domain grain-size range in magnetite and titanomagnetite. *J. Geophys. Res.*, 80:4049-4058.
- Cisowski, S., 1980. The relationship between the magnetic properties of terrestrial igneous rocks and the composition and internal structure of their component Fe-oxide grains. *Geophys. J. R. Astron. Soc.*, 60:107-122.
- Collot, J.-Y., Greene, H.G., Stokking, L.B., et al., 1992. *Proc. ODP, Init. Repts.*, 134: College Station, TX (Ocean Drilling Program).
- Day, R., Fuller, M., and Schmidt, V.A., 1977. Hysteresis properties of titanomagnetites: grain-size and compositional dependence. *Phys. Earth Planet. Inter.*, 13:260-267.
- Dunlop, D.J., 1969. Hysteretic properties of synthetic and natural monodomain grains. *Philos. Mag.*, 19:329-338.
- , 1981. The rock magnetism of fine particles. *Phys. Earth Planet. Inter.*, 26:1-26.
- Fisher, M.A., Collot, J.-Y., and Smith, G.L., 1986. Possible causes for structural variation where the New Hebrides island arc and the d'Entrecasteaux zone collide. *Geology*, 14:951-954.
- Haggerty, S.E., 1970. Magnetic minerals in pelagic sediments. *Year Book—Carnegie Inst. Wash.*, 68:332.
- Heider, F., Dunlop, D.J., and Soffel, H.C., 1992. Low-temperature and alternating field demagnetization of saturation remanence and thermoremanence in magnetite grains (0.037 μm to 5mm). *J. Geophys. Res.*, 97:9371-9381.
- Henshaw, R.C., Jr., and Merrill, R.T., 1980. Magnetic and chemical changes in marine sediments. *Rev. Geophys. Space Phys.*, 18:483-504.
- Hounslow, M.W., 1990. Grain fabric measured using magnetic susceptibility anisotropy in deformed sediments of the Barbados Accretionary Prism: Leg 110. In Moore, J.C., Mascle, A., et al., *Proc. ODP, Sci. Results*, 110: College Station, TX (Ocean Drilling Program), 257-275.
- Hrouda, F., 1982. Magnetic anisotropy of rocks and its application in geology and geophysics. *Geophys. Surv.*, 5:37-82.
- Johnson, H.P., and Hall, J.M., 1978. A detailed rock magnetic and opaque mineralogy study of the basalts from the Nasca Plate. *Geophys. J. R. Astron. Soc.*, 52:45-64.
- Johnson, H.P., Lowrie, W., and Kent, D.V., 1975. Stability of anhysteretic remanent magnetization in fine and coarse magnetite and maghemite particles. *Geophys. J. R. Astron. Soc.*, 41:1-10.
- Karlin, R., 1990. Magnetic mineral diagenesis in suboxic sediments at Bettis Site W-N, NE Pacific Ocean. *J. Geophys. Res.*, 95:4421-4436.
- King, J., Banerjee, S.K., Marvin, J., and Özdemir, Ö., 1982. A comparison of different magnetic methods for determining the relative grain size of magnetite in natural materials: some results from lake sediments. *Earth Planet. Sci. Lett.*, 59:404-419.
- Kronke, L.W., Jouannic, C., and Woodward, P. (Compilers), 1983. Bathymetry of the southwest Pacific, Chart 1: *Geophysical Atlas of the Southwest Pacific*, Scale 1:6,442,192 at 0°, Suva, Fiji. U. N. Econ. Soc. Comm. Asia Pac., CCOP/SOPAC Tech. Sec.

* Abbreviations for names of organizations and publications in ODP reference lists follow the style given in *Chemical Abstracts Service Source Index* (published by American Chemical Society).

- Levi, S., and Merrill, R.T., 1976. A comparison of ARM and TRM in magnetite. *Earth Planet. Sci. Lett.*, 32:171–184.
- Lowrie, W., and Fuller, M., 1971. On the alternating field demagnetization characteristics of multidomain thermoremanent magnetization in magnetite. *J. Geophys. Res.*, 76:6339–6349.
- Mallick, D.I.J., and Greenbaum, D., 1977. *Geology of Southern Santo*. Reg. Rep.—New Hebrides Condominium Geol. Surv.
- McNeill, D.F., 1990. Biogenic magnetite from surface Holocene carbonate sediments, Great Bahama Bank. *J. Geophys. Res.*, 95:4363–4371.
- Mitchell, A.H.G., and Warden, A.J., 1971. Geological evolution of the New Hebrides island arc. *J. Geol. Soc. London*, 127:501–529.
- Moon, T., and Merrill, R.T., 1986. Magnetic screening in multidomain material. *J. Geomagn. Geoelectr.*, 38:883–894.
- O'Reilly, W., 1984. *Rock and Mineral Magnetism*; New York (Chapman and Hall).
- Owens, W.H., 1993. Magnetic fabric studies of samples from Hole 808C, Nankai Trough. In Hill, I.A., Taira, A., Firth, J.V., et al., *Proc. ODP, Sci. Results*, 131: College Station, TX (Ocean Drilling Program), 301–310.
- Petersen, N., von Dobeneck, T., and Vali, H., 1986. Fossil bacterial magnetite in deep-sea sediments from the South Atlantic Ocean. *Nature*, 320:611–615.
- Sager, W.W., and Hall, S.A., 1990. Magnetic properties of black mud turbidites from ODP Leg 116, Distal Bengal Fan, Indian Ocean. In Cochran, J.R., Stow, D.A.V., et al., *Proc. ODP, Sci. Results*, 116: College Station, TX (Ocean Drilling Program), 317–336.
- Soffel, H.C., 1971. The single-domain/multidomain transition in intermediate titanomagnetites. *J. Geophys.*, 37:451–470.
- Stacey, F.D., and Banerjee, S.K., 1974. *Developments in Solid Earth Geophysics* (Vol. 5): *The Physical Principles of Rock Magnetism*; Elsevier (New York).
- Stoner, E.C., and Wohlfarth, E.P., 1948. A mechanism of magnetic hysteresis in heterogeneous alloys. *Philos. Trans. R. Soc. London A*, 240:599.
- Sugiura, N., 1979. ARM, TRM and magnetic interactions: concentration dependence. *Earth Planet. Sci. Lett.*, 42:451–455.
- Tarling, D.H., 1983. *Palaeomagnetism, Principles and Applications in Geology, Geophysics and Archaeology*; London (Chapman and Hall).
- Thompson, R., and Oldfield, F., 1986. *Environmental Magnetism*; London (Allen and Unwin).
- Xu, S., and Dunlop, D.J., 1993. Theory of alternating field demagnetization of multidomain grains implications for the origin of pseudo-single domain remanence. *J. Geophys. Res.*, 98:4183–4190.
- Xu, S., and Merrill, R.T., 1990. Toward a better understanding of magnetic screening in multidomain grains. *J. Geomagn. Geoelectr.*, 42:637–652.

Date of initial receipt: 14 May 1992

Date of acceptance: 2 September 1993

Ms 134SR-026

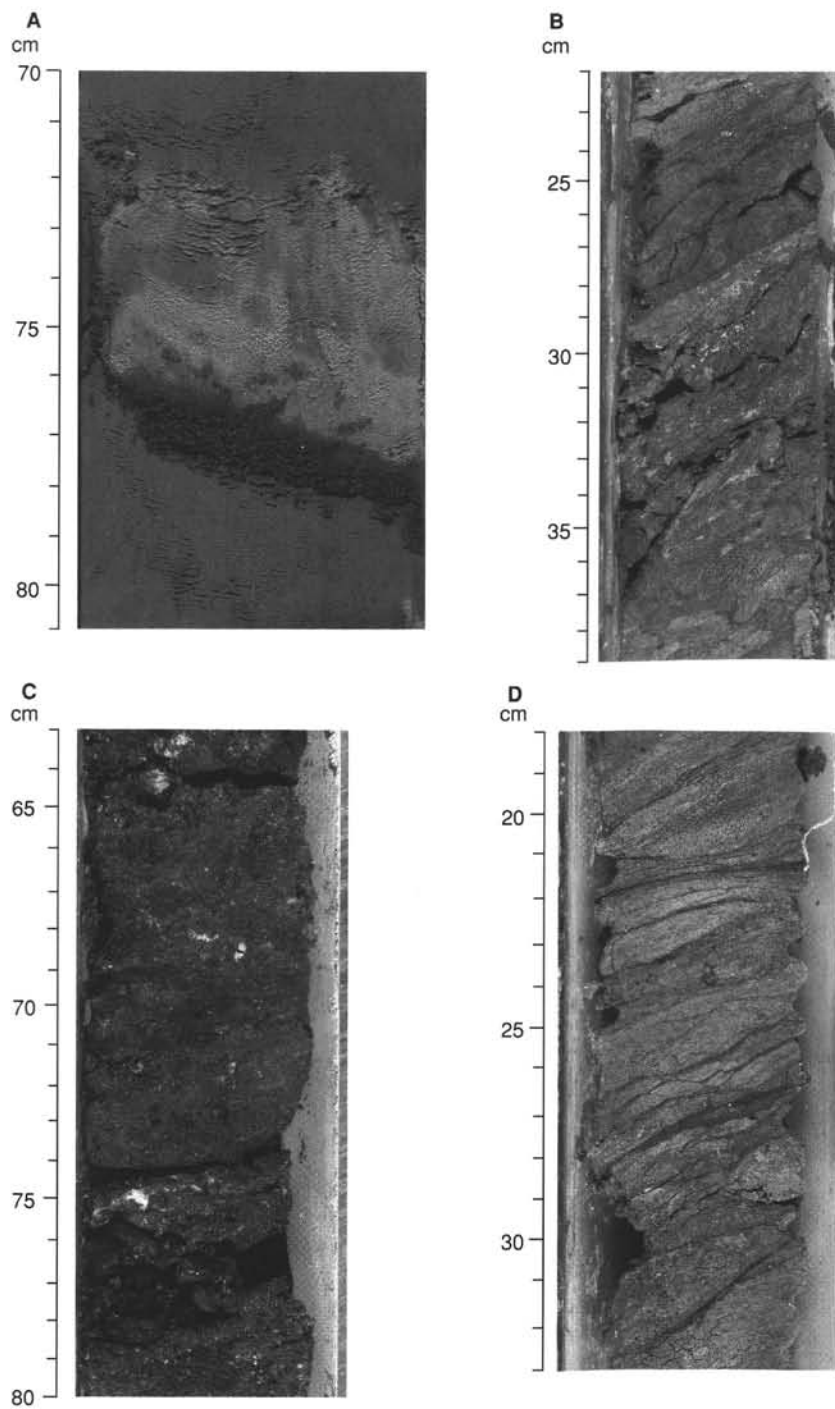


Plate 1. Core photographs illustrating typical sediments and rocks from Leg 134. A. Volcanic siltstone with ash layer (Interval 134-830A-3H-3, 70–81 cm). B. Deformed breccia (Interval 134-829A-43R-1, 22–39 cm). C. Volcanic sandstone (Interval 134-830C-7R-1, 63–80 cm). D. Chalk (Interval 134-829A-51R-1, 18–33 cm).

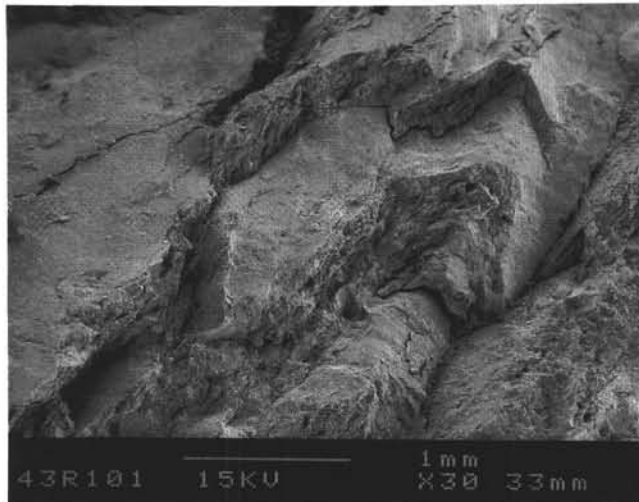
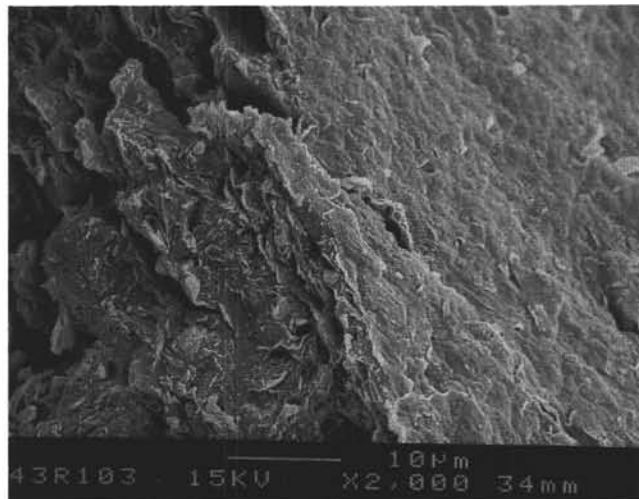
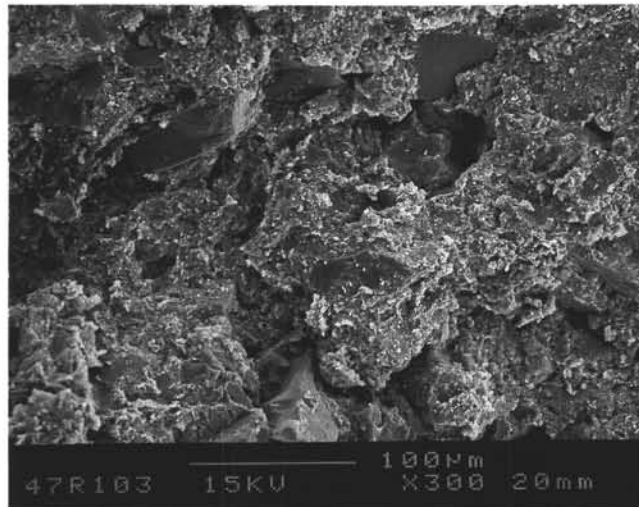
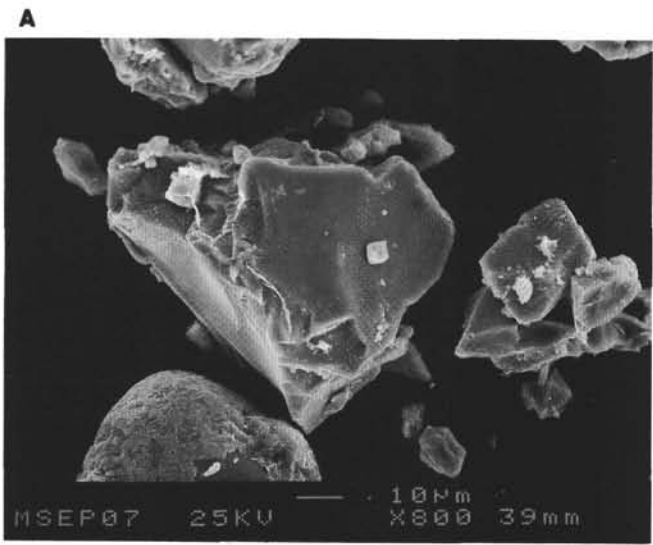
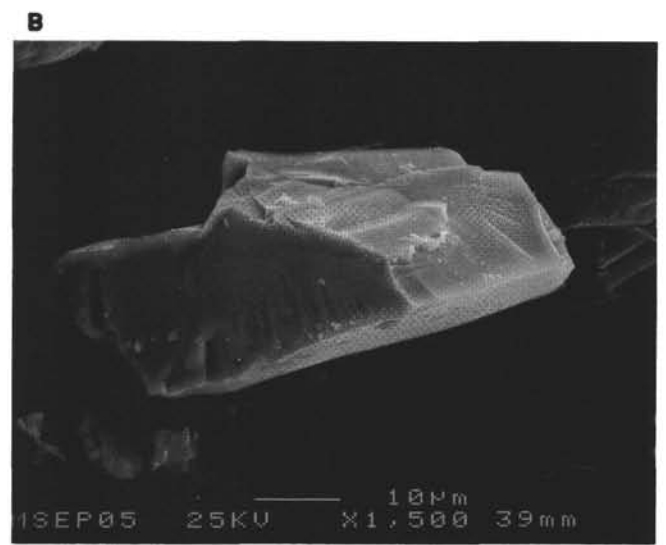
A**B****C**

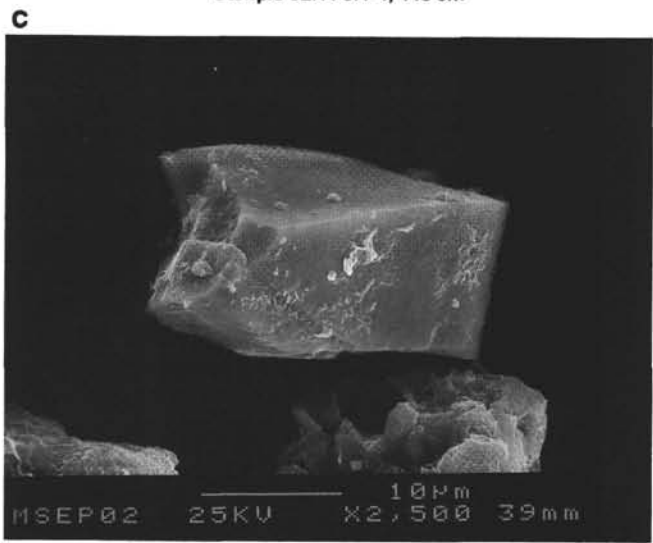
Plate 2. SEM photomicrographs illustrating the fabric of shear-zone samples. **A.** Sample 134-829A-43R-1, 144–146 cm, described in Collot, Greene, Stokking, et al. (1992) as a highly deformed breccia. The scale bar is 1 mm. **B.** Region in center of right flank of fold in upper-right corner of A. Scale bar is 10 μ m. **C.** Sample 134-829A-47R-1, 55–57 cm, a brown volcanic clay in which wavy lamina were observed (Collot, Greene, Stokking, et al., 1992). The scale bar is 100 μ m.



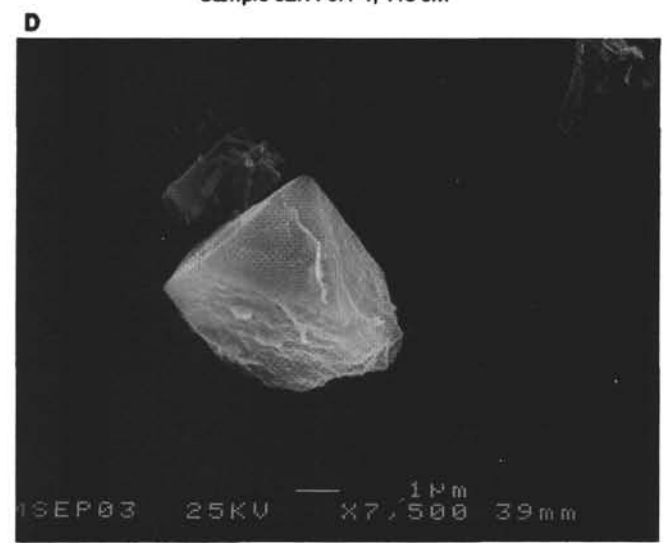
Sample 827A-9H-1, 118 cm



Sample 827A-9H-1, 118 cm



Sample 829A-6R-4, 110 cm



Sample 829A-6R-4, 110 cm

Plate 3. SEM photomicrographs illustrating titanomagnetites separated from volcanic silts. A, B. Sample 134-827A-9H-1, 118 cm. C, D. Sample 134-829A-6R-4, 110 cm.